Bull Volcanol (1996) 57:602–630

ORIGINAL PAPER

T. L. Wright · R. T. Helz

Differentiation and magma mixing on Kilauea's east rift zone: a further look at the eruptions of 1955 and 1960. Part II. The 1960 lavas

Received: July 10, 1995 / Accepted: October 10, 1995

Abstract New and detailed petrographic observations, mineral compositional data, and whole-rock vs glass compositional trends document magma mixing in lavas erupted from Kilauea's lower east rift zone in 1960. Evidence includes the occurrence of heterogeneous phenocryst assemblages, including resorbed and reversely zoned minerals in the lavas inferred to be hybrids. Calculations suggest that this mixing, which is shown to have taken place within magma reservoirs recharged at the end of the 1955 eruption, involved introduction of four different magmas. These magmas originated beneath Kilauea's summit and moved into the rift reservoirs beginning 10 days after the eruption began. We used microprobe analyses of glass to calculate temperatures of liquids erupted in 1955 and 1960. We then used the calculated proportions of stored and recharge components to estimate the temperature of the recharge components, and found those temperatures to be consistent with the temperature of the same magmas as they appeared at Kilauea's summit. Our studies reinforce conclusions reached in previous studies of Kilauea's magmatic plumbing. We infer that magma enters shallow storage beneath Kilauea's summit and also moves laterally into the fluid core of the East rift zone. During this process, if magmas of distinctive chemistry are present, they retain their chemical identity and the amount of cooling is comparable for magma transported either upward or laterally to eruption sites. Intrusions within a few kilometers of the surface cool and crystallize to produce fractionated magma. Magma mixing occurs both within bodies of previously fractionated magma and when new magma intersects a preexisting reservoir. Magma is otherwise prevented from mixing, either by wall-rock septa or by differing thermal and density characteristics of the successive magma batches.

Key words Kilauea · Magma mixing · Magmatic temperatures · Glass composition · Basalt composition · Magmatic plumbing/storage/transport

Editorial responsibility: M. Carroll

T. L. Wright (✉)
Smithsonian Institution, National Museum of Natural History, NHB-119, Washington, DC 20560, USA

R. T. Helz
U.S. Geological Survey, 107 National Center, Reston, Virginia 22092, USA

Introduction

The 1955 and 1960 lavas, both of which were erupted on Kilauea's lower east rift zone (Fig. 1), are of great interest to volcanologists because of the light they shed on processes of magmatic storage, differentiation, magmatic resupply, and eruptive behavior in a rift environment. The 1960 lavas were erupted from reservoir(s) that were the source of the 1955 lavas and which were recharged in 1955 with relatively low-magnesia magma originating beneath Kilauea's summit (Wright and Fiske 1971; Helz and Wright 1992). A similar recharge occurred in 1960 involving more magnesian magma (Murata and Richter 1966; Wright and Fiske 1971). Because of the conceptual significance of these two eruptions, we have revisited the petrogenesis of their lavas.

We have observed several different kinds of magma mixing in the 1960 lavas. Mixing occurs between stored magmas (fractionated compositions in equilibrium with olivine + clinopyroxene + plagioclase) and more primitive magmas (in equilibrium with olivine only). Both magma components are evident petrographically even though one component may be volumetrically minor. Mixing can also occur within stored magmas ("self-mixing"). Mixing occurred penecontemporaneous with the 1960 eruption ("recent" mixing) and also earlier, probably dating from 1955.

We have made new calculations to quantify the compositional end members contributing to the composition of each hybrid 1960 lava. Changes in the propor-

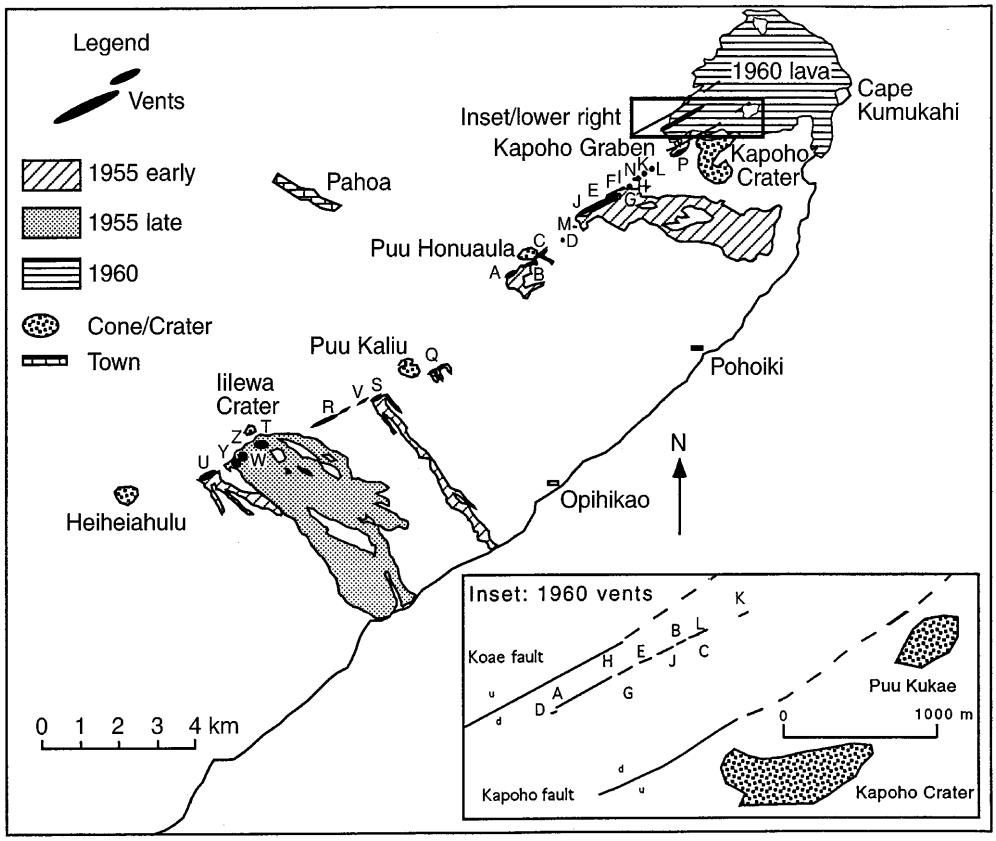

Fig. 1 Index map showing the lower part of Kilauea's east rift zone and vents and lava flows active in 1955 and 1960

tions of end members with time of eruption provides additional insight into the spatial and temporal continuity of Kilauea's magma reservoirs and pathways. Finally, we evaluate the thermal character of the magma reservoir that fed the 1955 and 1960 eruptions and propose a general model for magma transport and storage beneath Kilauea's east rift zone.

Magma mixing: general background and previous work at Kilauea

Many workers have contributed to the development of criteria for recognizing and quantifying magma mixing and hybridization in volcanic rocks. Classic studies of mixing in calc-alkalic systems include Eichelberger (1975) and Anderson (1976), among others. Mixing has also been recognized and evaluated in mid-ocean ridge basalts (e.g., Rhodes et al. 1979). In the absence of gross visible heterogeneity of the rocks, petrographic features which are commonly attributed to mixing include (a) hybrid phenocryst assemblages, with too many, or mutually incompatible, phases, (b) bimodal compositional ranges in minerals capable of continuous solid solution, (c) widespread occurrence of reversely zoned minerals, (d) widespread occurrence of resorbed crystals, and (e) occurrences of very disparate glasses as inclusions in phenocryst phases.

Recognition of the role that mixing and hybridization can play at basaltic volcanoes, such as Kilauea, has been more difficult because the effects of mixing and hybridization are subtler. Nevertheless, we believe that magma mixing is as important in this setting as elsewhere. It is appropriate to reevaluate the 1960 eruption because it was the first eruption at Kilauea recognized as having produced hybrid lavas.

The 1960 east rift eruption was originally described by Murata and Richter (Murata and Richter 1966; Richter and Murata 1966) who viewed it as essentially continuous with the 1959 summit eruption. These workers invoked magma mixing to explain petrographic and compositional features exhibited by the lavas produced in the middle of the eruption. They considered the earliest 1960 lavas to have been derived from magma left unerupted in 1955, but changes in the petrographic character and chemistry of the lavas erupted after 21 January led them to infer the existence of a second, hotter magmatic component in the later erupted lavas. The middle stages of the eruption were interpreted to be mixed magmas produced by combining the new and stored components.

Taking the observations of Richter and Murata on the 1960 eruption, along with additional data on the 1955 eruption, Wright and Fiske (1971) expanded on the idea of hybridization, offering a different hypothesis to explain the compositional shifts in both of these eruptions. Wright and Fiske proposed that several different batches of magma from Kilauea's summit were needed to produce the late 1960 lavas. Their study,

which used least-squares calculations, but which did not include petrographic and phase chemical data, provided permissive, but not conclusive, evidence for the process. A slightly later paper by Anderson and Wright (1972) interpreted textures and mineral and glass compositions as evidence for magma mixing in the early 1955 lavas, but did not look at the late 1955 or any of the 1960 lavas.

More recent studies documenting magma mixing effects at Kilauea include the work of Garcia et al. (1989, 1992) on the Puu Oo-Kupaianaha eruption, Clague et al. (1995) on samples from the submarine extension of Kilauea's east rift zone, and Helz and Wright (1992) on the late 1955 east rift lavas (Part I of the present study). A key feature of this previous study is our examination of glassy spatter samples, in preference to holocrystalline flow samples, in order to see pre-eruptive processes as clearly as possible.

Compositions and textures of early-formed minerals

The 1960 lavas contain phenocrysts of olivine, augite, and plagioclase. In addition we have observed rare, microphenocryst-sized crystals of hypersthene, which appear to be xenocrystic to their immediate hosts, and ilmenite, which occurs as an included phase in hypersthene. Again, as in Part I, we focus on the coarser, more texturally varied crystals in the samples investigated, because they record more prior history than smaller and/or homogeneous crystals. For this study we examined four samples of the early 1960 lavas (erupted 13–21 January 1960), three intermediate samples (erupted 22–30 January 1960), and seven late samples (erupted 2–18 February 1960); most of these are near-vent scoria and spatter.

Plagioclase

Representative compositions of plagioclase phenocrysts, microphenocrysts, and xenocrysts are tabulated in Table A1 and plotted in Fig. 2. The compositional range seen in the 1955 and 1960 lavas ($An_{51–80}$) is large, almost as large as the range ($An_{47.7–81.3}$) observed by Clague et al. (1995) in plagioclase phenocrysts in lavas from the entire submarine extension of Kilauea's east rift zone.

In the four early 1960 spatter samples, plagioclase phenocrysts are lath-like and mostly normally zoned, with few textural complications. One exception is a resorbed and moth-eaten crystal in KP-4 which shows some reverse zoning. Coarse phenocrysts are rare; the largest plagioclase observed in our sections is a crystal 4 mm in length in sample KP-8. Compositions of all plagioclase crystals (Fig. 2C) range from An_{76} to An_{56}; the maximum range observed in a single phenocryst is $An_{76–63}$. Microlites show a more restricted range ($An_{60.5}$ to $An_{65.0}$), reflecting the narrow range of melt compositions seen in these samples. The amount of phenocrystic and microphenocrystic plagioclase present in these samples is 9–10% by volume (data of Richter and Murata 1966).

Plagioclase phenocrysts in the late 1960 samples are almost all strongly resorbed (Fig. 3), as was also documented by Richter and Murata (1966, Fig. 6a, b) in their original description. The plagioclase phenocrysts are consistently calcic, ranging from An_{65} to An_{80} (Fig. 2). Calcic plagioclase in the late 1960 samples also occurs as inclusions in phenocrysts of iron-rich ($Fo_{76–78}$) olivine (see columns 7 and 10 in Table A1). Three of the latest samples examined have no phenocrystic or other early plagioclase at all; these are KP-25, the hot scoria in KP-26 (glass compositions in columns 3 and 4 in Table 1b), and KP-27, erupted from 13 February 1960 to 18 February 1960. The differentiated scoria in KP-26 (glass composition in column 5 in Table 1b) does contain phenocrystic plagioclase, which shows marked reverse zoning (columns 8 and 9 in Table A1). Richter and Murata (1966) show plagioclase phenocryst content declining from 4% in some intermediate samples to $<1\%$ in the late 1960 lavas, consistent with our observations.

Figure 2 also contains data on plagioclase phenocryst compositions from samples of the early and late 1955 lavas, including unpublished analyses of Ho and Garcia (1988), to facilitate comparison with the 1960 data. The range of observed compositions for plagioclase phenocrysts is quite large for both the early and late 1955 lavas, with compositions for plagioclase in the late 1955 lavas being clearly bimodal (Fig. 2B). The range in groundmass compositions in the early 1955 samples is $An_{55–61}$, which lies within the low end of the range of phenocryst compositions (Fig. 2A). The pattern of compositional data for plagioclase in the early 1955 lavas is thus similar to that of the early 1960 lavas. Although each has a continuous, rather than bimodal, range in plagioclase phenocryst compositions, the groundmass plagioclase falls *within* the range of phenocryst compositions, rather than extending below it. This implies that neither end of the phenocryst range is in equilibrium with the observed liquids in these samples.

Pyroxenes

Augite is the only pyroxene phenocryst present in the 1960 lavas, whereas the more magnesian late 1960 lavas contain larger crystals of both augite and hypersthene. Representative pyroxene compositions (Table A2) cover the range of composition previously observed in east rift lavas (Anderson and Wright 1972; Clague et al. 1995).

In the early 1960 lavas, augite phenocrysts (typically 1–2 mm in length) are common (6–7% by volume, according to Richter and Murata 1966). In some of the earliest samples (KP-4, KP-35) augite is deep olive-

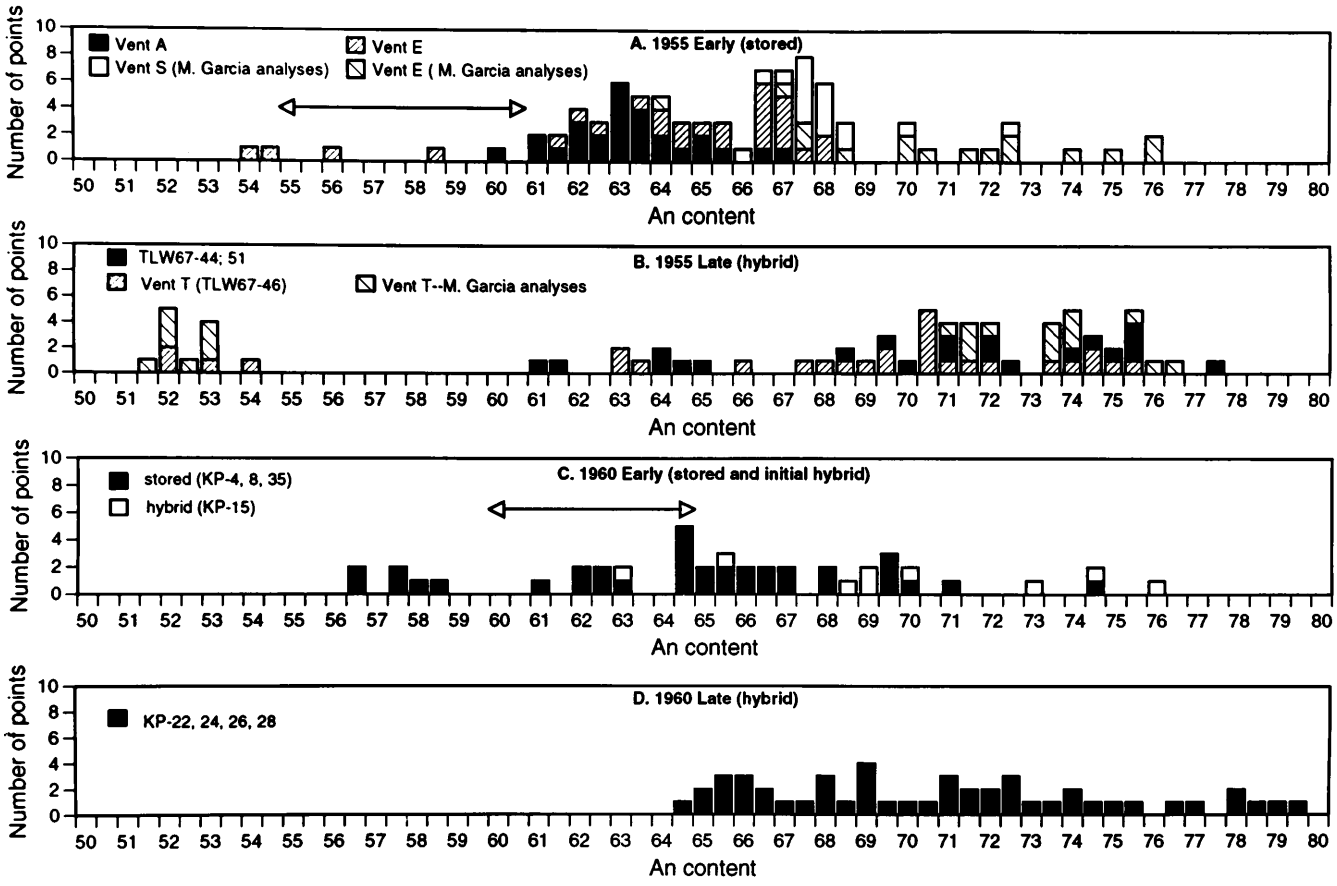

Fig. 2A–D Plagioclase compositions observed in samples from the early and late parts of the 1955 and 1960 eruptions. Each symbol corresponds to a single analyzed point. *Arrows* on early 1955 and early 1960 plots show range of microlite compositions

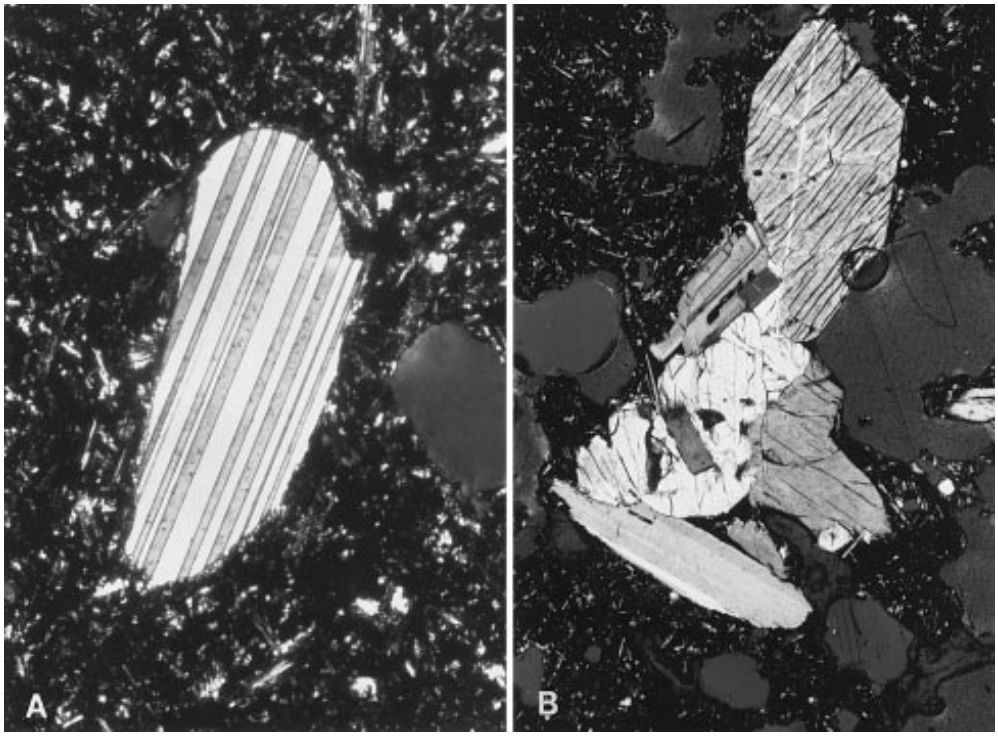

Fig. 3A, B Effects of magma mixing on plagioclase in late 1960 lavas. **A** Resorbed plagioclase phenocryst in sample KP-22, erupted on 4 February 1960. The grain is 0.5 mm long, with the composition shown in column 3 in Table A1. Nicols partly crossed. **B** Clump of augite + plagioclase microphenocrysts in same sample, showing different extent of resorption on plagioclase and augite. Aggregate is 2 mm across

Table 1a Composition of glasses from spatter samples from the early and middle parts of the 1960 eruption

Column no.	1	2	3	4	5	6	7	8	9	10
Field no.	KP-4	KP-49	KP-35	KP-35	KP-7	KP-8	KP-15	KP-16	KP-19	KP-19g
Date erupted	1/17/60	1/17/60	1/17/60	1/17/60	1/21/60	1/21/60	1/29/60	1/29/60	2/1/60	2/1/60
	Early (stored)	Early (stored)	Early (stored)	Early (stored)	Early (stored)	Early (stored)	Late (hybrid)	Late (hybrid)	Late (hybrid)	Late (hybrid)
No. of points	6		4	10	9	8	7	8	8	
SiO_2	50.7	50.95	50.6	50.6	50.4	50.4	50.8	50.4	50.5	50.62
TiO_2	3.66	3.58	3.61	3.62	3.68	4.24	3.59	3.16	3.17	2.96
Al_2O_3	13.4	13.58	13.4	13.4	13.5	12.4	13.2	13.9	13.8	14.05
Cr_2O_3	0.00	–	0.00	0.00	0.00	0.00	0.01	0.03	0.01	–
ΣFeO[a]	12.6	12.44	12.5	12.4	12.4	13.7	12.4	11.5	11.4	11.24
MnO	0.24	0.18	0.20	0.20	0.19	0.19	0.20	0.16	0.17	0.17
MgO	5.24	5.77	5.42	5.49	5.57	5.00	5.90	6.15	6.21	6.74
CaO	9.56	9.77	9.71	9.82	9.84	9.38	9.99	10.74	10.72	10.84
Na_2O	3.12	2.61	2.78	2.77	2.77	2.64	2.69	2.69	2.55	2.49
K_2O	0.81	0.72	0.77	0.77	0.76	0.90	0.73	0.66	0.66	0.59
P_2O_2	0.37	0.39	0.38	0.36	0.39	0.48	0.35	0.28	0.28	0.30
Sum	99.88	100.00[b]	99.17	99.43	99.50	99.33	99.86	99.67	99.47	100.00[b]
TMgO	1122		1122	1123	1125	1113	1133	1137	1138	
Comments				Replicate analysis		Abundant crystallites in glass				
Murata and Richter no.	F-3	F-3g	–	–	F-5	F-6	F-8	–	F-11	F-11g
USNM no.	116112.03		116112.34		116112.06	116112.07	116112.14	116112.15	116112.18	

[a] Total iron as FeO
[b] Glass analyses from Murata and Richter (1966), with all iron as FeO, renormalized to 100%

Table 1b Composition of glasses from spatter samples from the late 1960 eruption

Column no.	1	2	3	4	5	6	7	8
Field no.	KP-25	KP-25	KP-26	KP-26	KP-26	KP-27	KP-27	KP-27g
Date erupted	2/13/60	2/13/60	2/16/60	2/16/60	2/16/60	2/18/60	2/18/60	2/18/60
	Late (hybrid)	Late (hybrid)	Late (hybrid)	Late (hybrid)	Late (hybrid)	Late (hybrid)	Late (hybrid)	Late (hybrid)
No. of points	8	5	4	7	4	6	10	
SiO_2	50.6	50.5	50.6	50.6	50.8	51.1	51.3	50.59
TiO_2	2.97	3.01	3.01	3.00	3.44	3.00	3.03	2.96
Al_2O_3	13.9	13.9	13.9	13.9	13.6	13.6	13.8	13.97
Cr_2O_3	0.03	0.01	0.00	0.00	0.02	0.00	–	
ΣFeO[a]	10.9	10.8	10.9	10.9	12.0	11.0	11.0	11.0
MnO	0.18	0.17	0.24	0.17	0.18	0.17	0.16	0.17
MgO	6.48	6.47	6.45	6.42	5.76	6.40	6.39	6.97
CaO	11.12	11.09	10.83	10.93	9.96	11.02	10.97	10.81
Na_2O	2.57	2.69	2.74	2.72	2.79	2.80	2.74	2.54
K_2O	0.59	0.63	0.65	0.64	0.74	0.64	0.65	0.60
P_2O_5	0.27	0.26	0.28	0.26	0.32	0.30	0.27	0.30
Sum	99.61	99.53	99.61	99.54	99.41	100.05	100.31	100.00
TMgO	1144	1144	1143	1142	1129	1142	1142	
Comments		Replicate analysis	Scoria 1	Scoria 2	Scoria 3 differentiated			
Murata and Richter no.	F-17	F-17	F-18	F-18	F-18	F-19	F-19	F-19g
USNM no.	116112.24		116112.25			116112.26		

[a] Total iron as FeO
[b] Glass analyses from Murata and Richter (1966), with all iron as FeO, renormalized to 100%

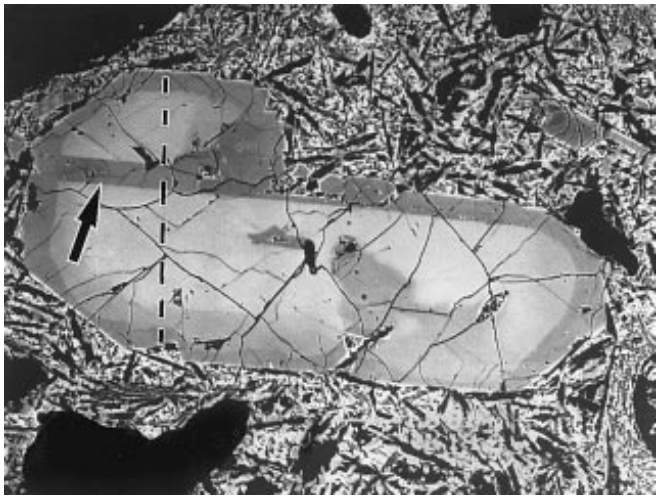

Fig. 4 Scanning electron microscopy (SEM) image of a compound pyroxene phenocryst in sample KP-24. This 1-mm-long grain consists of a thick blade of hypersthene, shown by *arrow,* surrounded by relatively Fe-rich augite. This core has undergone two distinct episodes of partial resorption, followed by growth of a more Mg-rich rim. The microprobe traverse shown in Fig. 5 is shown by a *dashed line.* Compositions of the different parts of this grain are given in columns 7–10 in Table A2

green in color; in most other samples it is brownish, but still fairly strongly colored. In contrast to the early 1955 lavas, where the green augite is distinctly more ferroan (Anderson and Wright 1972; Table 2) than the pale augite found in the same samples, the differently colored augites in the early 1960 lavas do not have different compositions. Zoning, which can be either normal or reverse, is dominated by the Ca–Fe exchange, without large changes in MgO content. The zoned crystals (Table A2) show a substantial increase in Cr in the Fe-poor rims, consistent with the interpretation that this is reverse zoning, even though the MgO content of the rims is similar to that of the cores.

Augite phenocrysts in the later 1960 lavas are still abundant (3–5% according to Richter and Murata 1966), and unlike plagioclase, rarely have resorbed outlines. The contrast between euhedral augite and resorbed plagioclase in an augite–plagioclase clot is shown in Fig. 3B. More detailed examination of augite phenocrysts, involving electron-microprobe traverses and scanning electron microscopy (SEM) imaging, has revealed complex histories of multiple episodes of resorption and/or reverse zoning in individual augite phenocrysts, even those with euhedral outlines.

A compound phenocryst from sample KP-24 (Fig. 4) illustrates some of the complexities found in pyroxene phenocrysts from the stored magma. It consists of a thick lamella of hypersthene surrounded by relatively bright Fe-rich augite (column 7 in Table A2). The ragged outline of the Fe-rich augite is surrounded by a somewhat more magnesian augite (column 8 in Table A2) which fills in the deepest embayments. That zone is mostly euhedral, but with some local resorption, and is in turn surrounded by a distinctly darker rim of much more magnesian and Cr-rich augite (column 9 in Table A2) which gives the grain its present euhedral outline against the groundmass. A microprobe traverse across the left side of the grain (Fig. 5) shows the two stages of reverse zoning in more detail.

The sector-zoned augite shown in Fig. 6 also shows a complex history, even though it originated in a hotter recharge component. The sectors in this crystal differ at both major- and minor-element levels, as can be seen in the microprobe traverse shown in Fig. 7. The small dark trapezoidal area near the core (column 12 in Table A2) is subcalcic augite like that found in a sector-zoned augite in one of the late 1955 lavas (Helz and Wright 1992, Fig. 4e). This composition is metastable, plotting within the pyroxene solvus as defined by Ross and Huebner (1979). The remainder of the dark sector (the part that is inclusion-ridden) is augite with Ca, Mg, and Fe contents very similar to those of the lighter, dominant sectors, but with Al and Ti contents like those of the metastable, subcalcic augite. The sectored core has been slightly resorbed around its edge; the darker, slightly more magnesian augite rim truncates the sectoring, and is uniform in composition around the crystal (see Fig. 7). Clearly, this grain records an initial large departure from equilibrium, and has had a fairly complicated subsequent history as well. (Not all sectored augite in the late 1960 lavas is complex; the analyses in columns 18 and 19 in Table A2 are from a sectored augite phenocryst where there is no compositional difference between sectors. In this crystal the sectoring must be due to slight differences in orientation of the crystal lattice only, and the departure from equilibrium during its growth is slight.)

Hypersthene as a phenocrystic mineral is rare at Kilauea. It is fairly common in the early 1955 lavas (Macdonald and Eaton 1964; Anderson and Wright 1972), but has not been observed in the late 1955 samples. It was reported by Richter and Murata (1966) as rare in the early 1960 lavas, detected only in heavy-mineral separates; none occurs in any of our sections. However, we have found hypersthene in two of the late 1960 samples, where it has not been observed previously.

Hypersthene in the late 1960 lavas has a uniform composition (Table A2), but its textural relationship to the host varies. The thick blade of hypersthene enclosed in the complexly zoned augite described above (Fig. 4) is in equilibrium with the adjacent Fe-rich augite (columns 6 and 7 in Table A2). Hypersthene also occurs as clusters of microphenocryst-sized, resorbed crystals surrounded by thin rims of magnesian augite (Fig. 8A; analyses in columns 3 and 4 in Table A2); the rims are not, in this case, in equilibrium with the hypersthene. One hypersthene crystal (Fig. 8A) contains an inclusion of ilmenite (column 5 in Table A2). The presence of the ilmenite inclusion, and the iron-rich character of the hypersthene itself, confirm that these crystals have come from a fractionated source. Hyper-

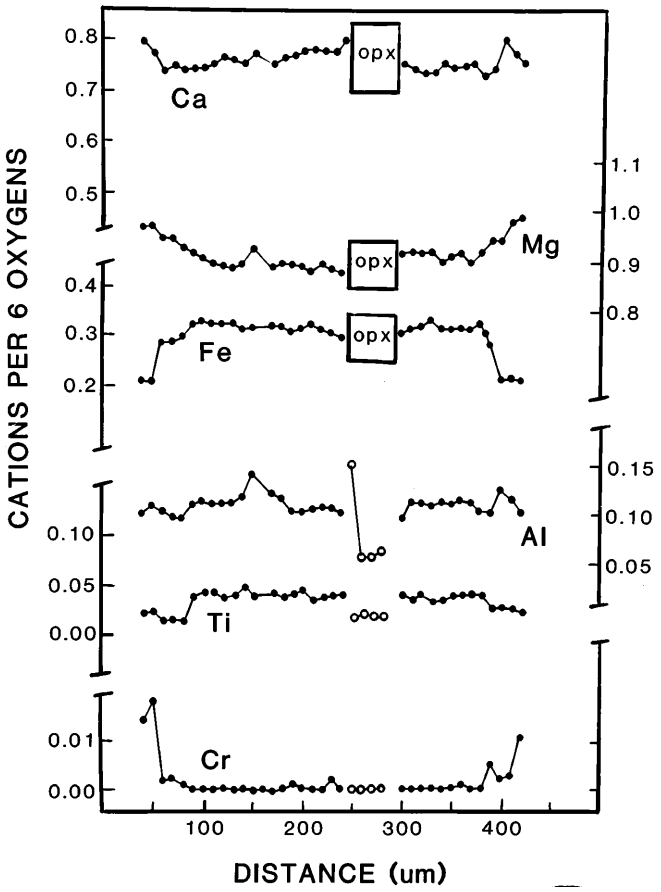

Fig. 5 Microprobe traverse of compound pyroxene shown in Fig. 4. The Fe, Ti, and Cr profiles show best the two distinct rims along the upper edge of the grain. Ca, Mg, and Fe for the opx lamella have been omitted from this figure because they plot off-scale, but the Al and Ti data show the contrast between the minor-element concentrations in opx and augite

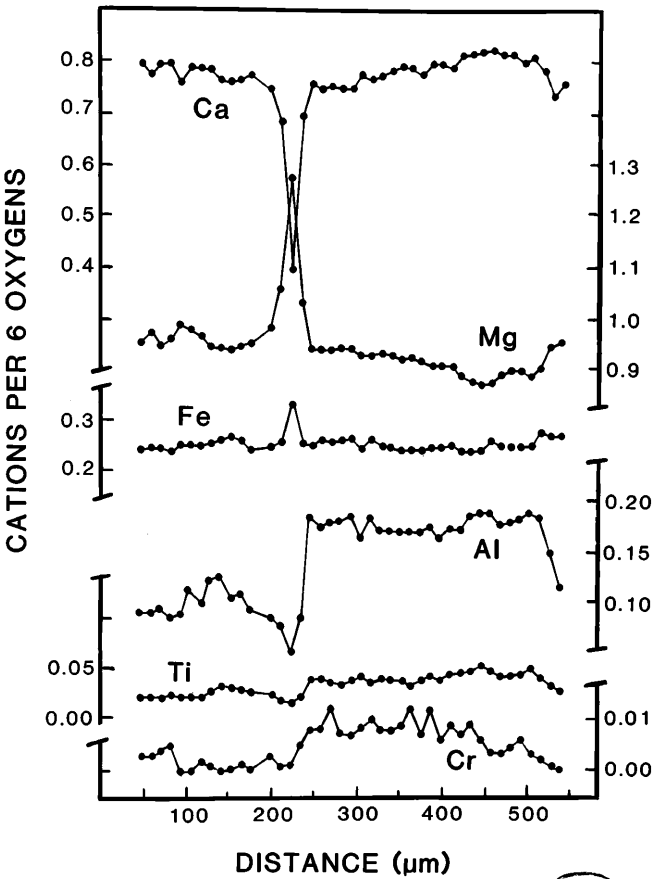

Fig. 7 Microprobe traverse of the sector-zoned augite shown in Fig. 6. Note the contrast in Al, Ti, and Cr contents of the augite in the dark sector vs the augite in the light sector. The extremely low-Ca cpx makes up only a very small region near the center of the grain

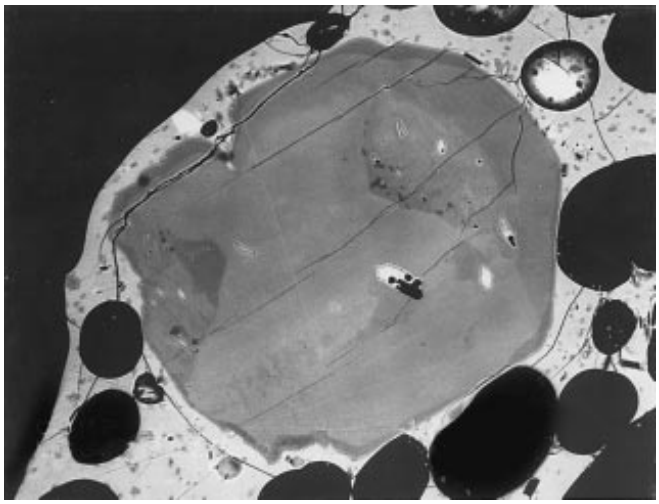

Fig. 6 SEM image of a sector-zoned augite microphenocryst in sample KP-25, erupted 13 February 1960. The crystal is 0.5 mm across. Compositions of different parts of this grain are given in columns 10–12 in Table 1b. The *arrows* indicate the orientation of the microprobe traverse shown in Fig. 7

sthene is present also in the piece of differentiated scoria in sample KP-26. It is in direct contact with the melt, but is not in equilibrium with the melt or with any of the augite present in the same glass (columns 14–16 in Table A2).

Olivine

Olivine is the most abundant phenocrystic phase in the 1960 lavas. In early 1960 lavas, olivine is relatively small (<2 mm in length) and sparse (1–2% by volume according to Richter and Murata 1966), euhedral in form and normally zoned (columns 1 and 2 in Table A3). The late 1960 lavas have abundant olivine phenocrysts (5–14% by volume according to Richter and Murata 1966), with a variety of core compositions (Fig. 9), zoning patterns (Fig. 10), and textures (Figs. 11–12), which provide vivid documentation of recent magma mixing in the chamber from which the lavas were erupted.

Core compositions (Fig. 9) range from Fo_{76} to Fo_{88}, and fall into three compositional groups. These proba-

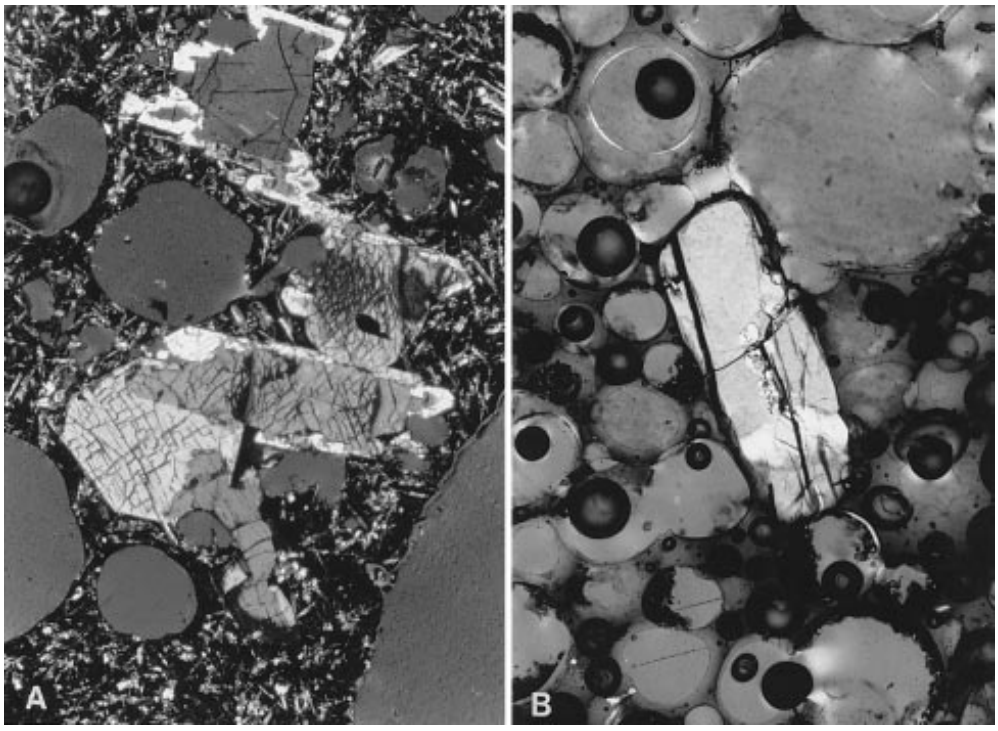

Fig. 8A, B Occurrence of hypersthene in the 1960 lavas. **A** Cluster of hypersthene crystals with thin rims of magnesian augite, in sample KP-24, erupted on 12 February 1960. One hypersthene grain contains an inclusion of ilmenite. Phase compositions given in columns 3–5 in Table A2. Cluster is 1.5 mm across. **B** Hypersthene crystal (1 mm long) in differentiated scoria in sample KP-26, erupted 16 February 1960. The grain, the composition of which is given in column 14 in Table A2, is resorbed, but lacks any augite rim

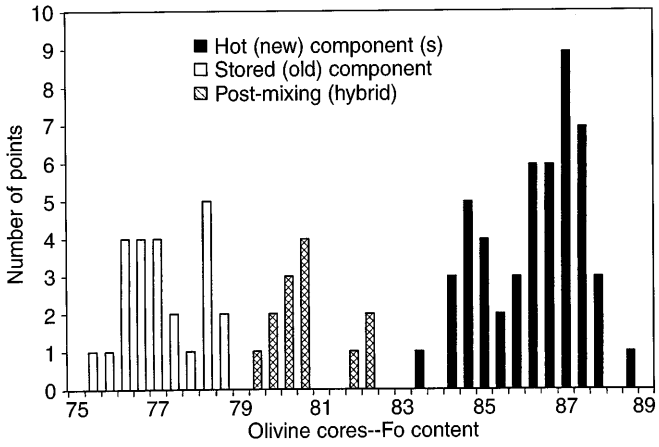

Fig. 9 Frequency distribution of core compositions of olivine phenocrysts, microphenocrysts, and xenocrysts in the 1960 lavas. Includes some data from early sample KP-4, as well as from the late samples. The data fall into three groups corresponding to cooler magma stored in the rift, hotter magma introduced from Kilauea's summit, and the magma hybridized by mixing

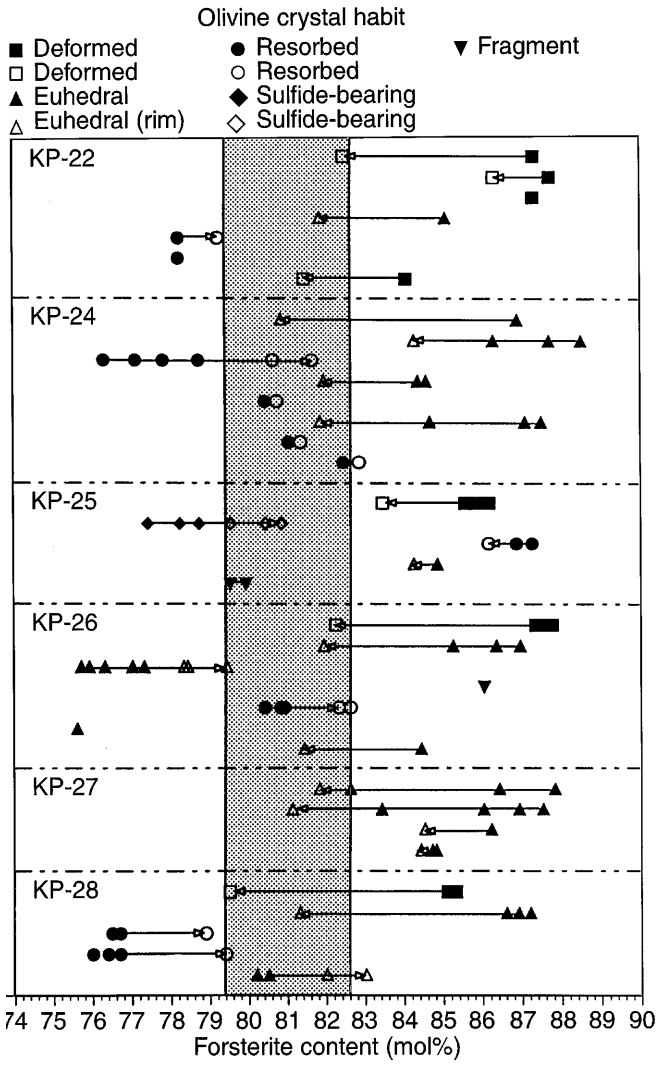

Fig. 10 Olivine zoning in samples of the late 1960 lavas (*solid symbols* core compositions; *open symbols* rim composition). The two *vertical lines* bracket the range of initial olivine compositions which would be in equilibrium with the liquid at the first appearance of plagioclase, assuming that the distribution for Fe–Mg exchange between olivine and liquid is 0.27–0.30 (Roeder and Emslie 1970). Olivine compositions lying to the right or left of this band must have crystallized from more Mg-rich or less Mg-rich liquids, respectively. Note that grains with core compositions lying outside the vertical lines are zoned toward intermediate compositions

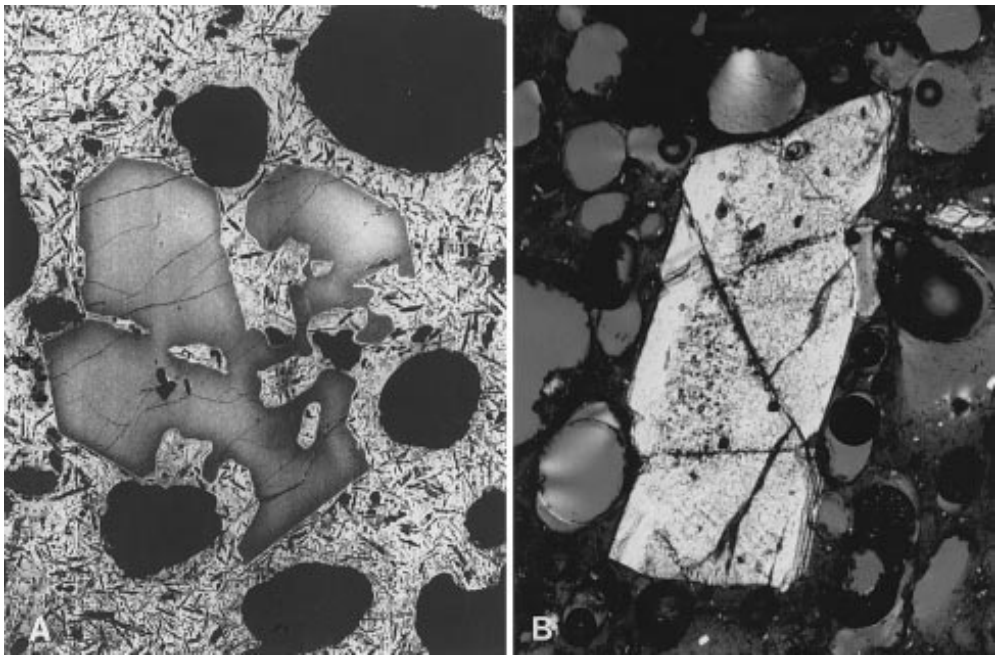

Fig. 11A, B Olivines inherited from the stored component. **A** SEM image of a resorbed, reversely zoned olivine phenocryst in sample KP-24, erupted on 12 February 1960. This grain is relatively Fe-rich; this fact, plus the presence of plagioclase inclusions (*black polygonal areas* in core), and the absence of chromite inclusions all suggest that this grain crystallized from a differentiated magma. The grain is 1.2 mm across. **B** Inclusion-rich olivine fragment in sample KP-25, erupted 12 February 1960. The grain is 1.5 mm long and has been broken at both ends. It shows slight reverse zoning (compositions are given in columns 6 and 7 in Table A3). The inclusions are compound, containing glass + chromite ± sulfide + vapor. Crossed nicols

bly represent, from low to high Fo content, olivine crystallized from the stored component, olivine growing in the newly created hybrid magma, and olivine brought in with the various primitive components. The zoning patterns (Fig. 10) support this inference. Five of the six samples examined contain olivine phenocrysts with both Fe-rich and Mg-rich cores, neither of which were stable in the present (hybrid) melts. The zoning of these phenocrysts is toward a central range of olivine compositions. This range ($Fo_{79.5–82.5}$) corresponds to the olivine which would be stable at the melt MgO content where plagioclase begins to crystallize in Kilauean melts (approximately 7.0% MgO). Olivines with core compositions in this range are mostly unzoned; reversely zoned crystals in some of the latest samples may reflect repeated recharge of the chamber. Sample KP-27, the last pumice sample collected at the very end of the eruption, is completely free of phenocrysts of Fe-rich olivine, plagioclase, or augite.

The textures observed in the Fe-rich olivine phenocrysts (Fig. 11) confirm the inferences drawn from the distribution of core compositions and from zoning patterns. Figure 11A shows a very strongly resorbed grain with a cluster of included plagioclase grains. The core is Fe-rich (columns 4 and 5 in Table A3); the very narrow, more magnesian rim follows the elaborately resorbed outline of the grain, showing unequivocally that the reverse zoning postdates the resorption. The presence of plagioclase inclusions in this grain provides additional evidence that it grew in a relatively differentiated magma.

Figure 11B shows an elongate olivine grain with an inclusion-rich core and clear rims, approximately 30 mm thick, along its sides (compositions in columns 6 and 7 in Table A3). The rim has been locally resorbed, as can be seen by its curving upper contact. In one place along this side, the rim has been completely dissolved away, and the inclusion-rich core is in direct contact with the melt. All zoning is cleanly truncated at the broken ends of the fragment, showing that the breakage postdates the development of the reversely zoned rim, and (probably) the limited resorption observed along it. There is no differential resorption of the different zones along the broken surfaces, nor any development of more forsteritic rims on the core region exposed by the breaks, which suggests that the breakage is very recent. This grain thus shows evidence of two stages of hybridization and/or disruption in the magma chamber from which it was derived.

The very forsteritic olivines include euhedral crystals and deformed grains, irregular in form, with multiple extinction discontinuities. The latter occur singly or in aggregates, measuring up to 5 mm across (Fig. 12). Their core compositions range from Fo_{84} to Fo_{88}. These grains and aggregates are identical in appearance and in their compositional range to the large, blocky, deformed olivines and dunitic aggregates observed in the 1959 summit lavas and in Kilauea Iki lava lake. (Richter and Murata (1966) noted the coarse grain size and noneuhedral forms of olivine phenocrysts in both the 1959 and 1960 lavas, but did not mention deformation features in either. Olivines like this are also quite common in the submarine east rift lavas as stated in Clague et al. 1995.) Helz (1987a) interpreted the deformed, blocky olivines in the 1959 lavas as xenocrysts, and suggested that they were derived from olivine cumulates, precipitated from earlier Kilauean lavas, but now transected by Kilauea's current plumbing system, an idea generalized recently to apply to other Kilauean picrites (Clague and Denlinger 1994). We believe the coarse, deformed olivines in the late 1960 lavas have the same origin. The fact that their NiO contents cover the same

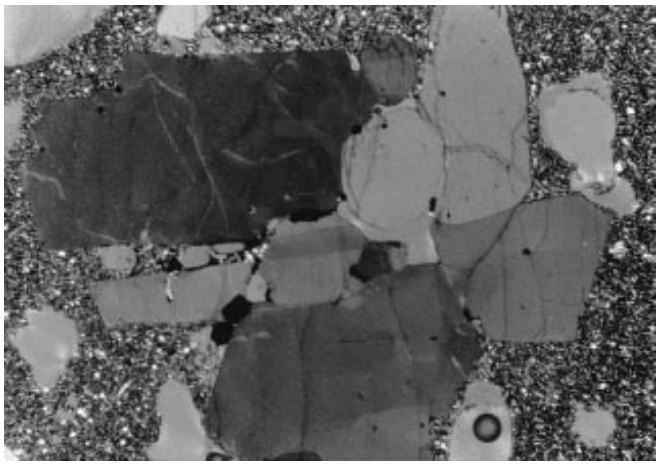

Fig. 12 Aggregate of mildly deformed olivine in sample KB-22. The aggregate is 5 mm across. Grains in the aggregate are forsteritic (composition given in column 3 in Table A3), except for a very thin rim next to the devitrified matrix, which reaches Fo 82.5 locally. All grains in the aggregate are deformed, and almost all coarse chromite (black) is found at grain boundaries within the aggregate, rather than as inclusions in the olivine. This aggregate very closely resembles the commonest type of olivine aggregate in the 1959 summit lavas (Fig. 5B and 7C in Helz 1987a)

range as those of the euhedral forsteritic phenocrysts present in the same samples (see Table A3) is consistent with this suggestion.

Chemical variation: whole-rock and glass compositions

Murata and Richter (1966) published major-oxide chemical analyses of lava samples collected during the eruption. Their data is reproduced in Table 2, with trace element data (Table A4) analyzed by nondispersive X-ray fluorescence as described in Part I (Helz and Wright 1992, p. 374ff). Selected major oxides (Al_2O_3, total iron such as FeO, CaO, and TiO_2) are plotted against MgO (Fig. 13A) and selected incompatible (Zr, Sr) and compatible (Cr, Ni) trace elements are also plotted against MgO (Fig. 13B). In addition, Fig. 13A shows the compositions from selected summit eruptions which occurred close to, both before and after, the 1960 east rift eruption. The lines extending back to 12% MgO are "olivine control" lines, which assume an average olivine phenocryst composition of Fo_{87}. Bulk compositions falling along such control lines have been observed in the 1959 lavas (Wright 1971; Wright 1973) and have been inferred to exist for other Kilauean magmas (Wright 1971).

As can be seen in Fig. 13A, the early 1960 lavas (samples erupted from 13 January through 21 January) have a limited range of compositions (MgO = 6.0–6.5%), similar to those of lavas erupted near the end of the 1955 eruption. The main difference between the early 1960 lavas and the late 1955 lavas is that the 1960 lavas are somewhat lower in FeO at a given MgO content. These samples define the "stored" component of the 1960 eruption. The MgO content of lava increases after 26 January, ranging between 7 and 13%.

The expected liquid line of descent for Kilauean compositions should follow the "olivine control" slope shown until three-phase fractionation begins at approximately 7.0% MgO. In two plots (those for CaO and FeO) the 1960 samples define slopes on the variation diagrams which deviate from olivine-only fractionation at MgO contents where multiphase fractionation is not possible [see Thompson and Tilley's (1969) experimental results on the crystallization behavior of the 1960 lavas]. In addition, for certain oxides the 1960 bulk compositions fall well outside the range defined by erupted Kilauean magmas or their inferred, more magnesian parents: In particular, TiO_2 is too high and CaO too low for the 1960 lavas to have been derived by fractionation of any known Kilauean parental lava.

Even more telling evidence for the hybrid nature of the 1960 lavas can be found in looking at the actual glass compositions found in these samples (shown in Table 1 and in Fig. 13A). The glass analyses were obtained as described in Part I (Helz and Wright 1992); quenching temperatures (T_{MgO}) are inferred using the calibration of Helz and Thornber (1987). Replicate analyses for several samples give some indication of the uncertainty in the analyses including both the analytical uncertainty and the effects of slight heterogeneity in the glasses. Most of the spatter samples analyzed were uniform in composition and texture, even when multiple lapilli were examined. Sample KP-26, however, contained two lapilli with hotter, less-differentiated glass (columns 3 and 4 in Table 1b) and a third fragment of cooler, more differentiated glass (column 5 in Table 1b). The difference between these glass compositions is analytically significant for all components.

The glass compositions unequivocally define the location of the liquid line of descent for the 1960 bulk compositions. Figure 13A shows that the whole-rock trends for the intermediate and late lavas diverge widely from that line. This is especially conspicuous in the plot of CaO vs MgO, where the glasses continue to show a positive correlation between the two oxides, with a peak at 11.2% CaO and 7.0% MgO, the point at which plagioclase begins to crystallize in Kilauean magmas. The whole-rock compositions, by contrast, show CaO peaking at $<10.5\%$ CaO. The divergence between melt and bulk-rock compositional trends is not peculiar to the microprobe analyses: Three wet-chemical analyses of glass separates from the 1960 eruption, presented by Murata and Richter (1966), and plotted in Fig. 13A for comparison, are similar to the microprobe analyses. (Their slightly higher MgO content most probably reflects the presence of very minor amounts of olivine in the glass separates.) These data provide unequivocal evidence that the later 1960 bulk compositional trends diverge widely from the true liquid line of descent of Kilauean liquids in general, and the 1960 equilibrium liquids in particular.

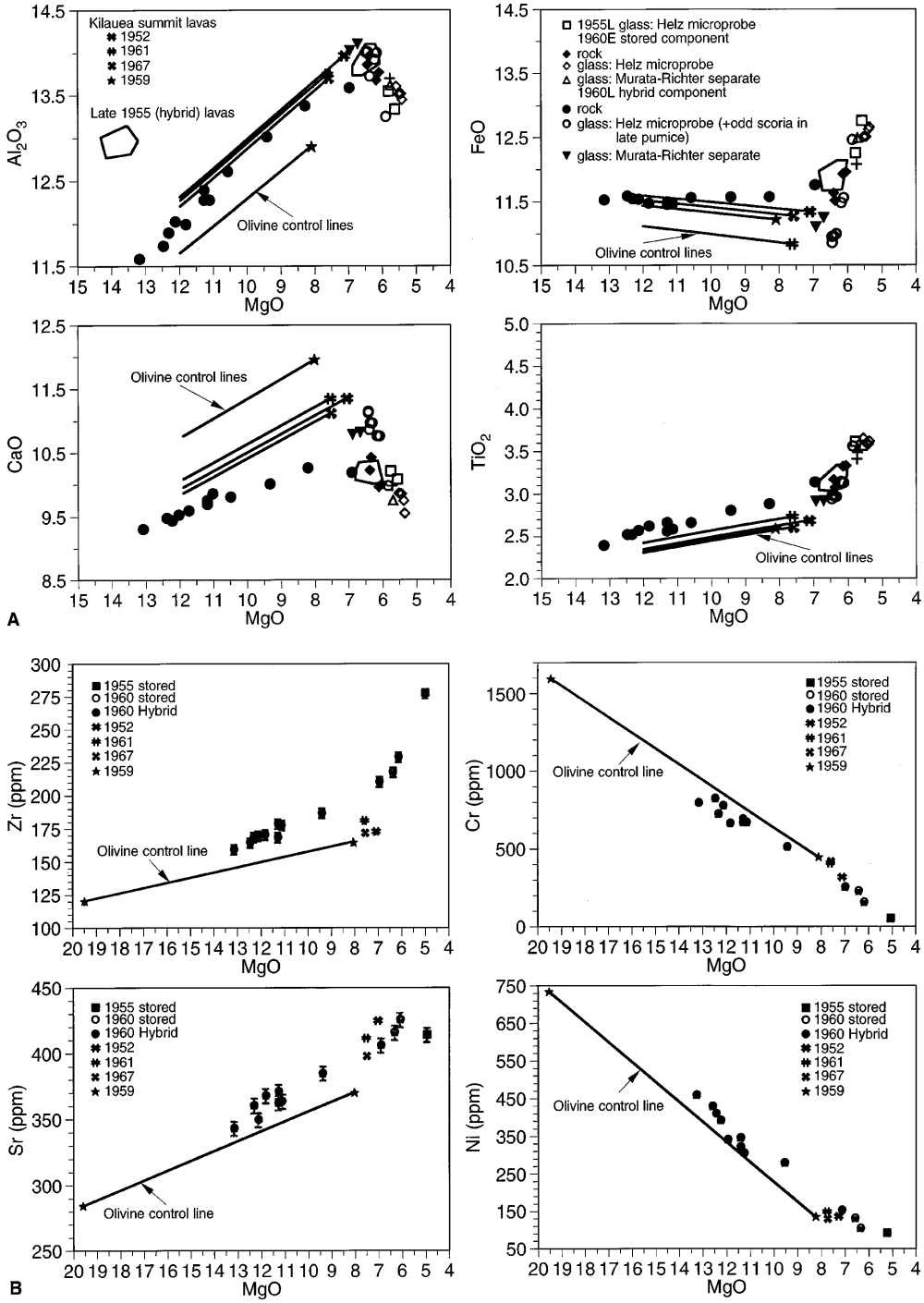

Fig. 13A, B Selected MgO variation diagrams. A representative liquid line of descent for Kilauean magmas extends from olivine control lines extrapolated to approximately 7.0% MgO and the 1955 glass (*open squares*). The 1960 lava compositions do not follow olivine control lines; instead, they can be modeled as a mixture of one or more compositions lying on a liquid line of descent with olivine-rich liquids falling on olivine control lines or their extrapolation to more magnesian compositions. **A** Al_2O_3, total iron as FeO, CaO, and TiO_2, showing relationships between glass and whole-rock compositions from the 1955 and 1960 eruptions. **B** Selected incompatible elements (Zr, Sr) and compatible (Cr, Ni) trace elements

Discussion: petrographic evidence for mixing in the 1960 lavas

The early 1960 lavas

All of the minerals present in the early lavas of Kilauea's 1960 east rift eruption record evidence for magma mixing, despite the great uniformity in the glass compositions in the samples investigated. This evidence includes the presence of reversely zoned augite and normally zoned olivine phenocrysts/microphenocrysts in the same sample (KP-4; columns 1 and 2 in Tables A2 and A3). The rim compositions from KP-4 are in equilibrium with each other, and are presumably in equilibrium with the present host melt (columns 1 and 2 in Table 1a). This implies that the core compositions of these same microphenocrysts are not in equilibrium with each other, and that neither core is in equilibrium with the host liquid. The narrowness of the zoned rims suggest that the mixing occurred very close to the time of eruption. The early 1960 lavas also contain resorbed, reversely zoned plagioclase microphenocrysts.

Table 2 Major-oxide[a] and trace element[b] data for samples from the 1960 eruption (F-1 to F-20) and from Kilauea's summit (1952–1967)

ID no.	F-1	F-6	F-7	F-9	F-11	F-12	F-13	F-14	F-16	F-17	F-18	F-19	F-20	1960E[c]	1952[c]	1961[c]	1967[c]	1959 S-1[c]
Field no.		KP-08	KP-13	KP-17	KP-19	KP-20	KP-21	KP-22	KP-24	KP-25	KP-26	KP-27	KP-28					
Eruption date	1/13	1/21	1/26	1/30	2/1	2/2	2/4	2/4	2/12	2/13	2/16	2/18	2/18					
SiO_2	50.68	50.98	50.58	49.74	49.37	49.48	49.02	49.30	49.18	48.95	49.44	49.04	49.27	50.8	50.32	50.38	50.45	50.10
Al_2O_3	13.91	13.64	13.55	12.99	12.38	12.60	12.02	12.27	11.89	11.59	12.27	11.74	11.99	13.77	13.91	13.70	13.65	12.88
FeO total	11.50	11.94	11.74	11.55	11.44	11.55	11.52	11.48	11.53	11.51	11.45	11.57	11.46	11.74	11.32	10.83	11.26	11.21
MgO	6.57	6.19	6.99	9.44	11.31	10.61	12.15	11.31	12.34	13.18	11.15	12.49	11.85	6.33	7.14	7.64	7.60	8.11
CaO	10.45	9.99	10.21	10.03	9.77	9.83	9.54	9.71	9.45	9.32	9.88	9.49	9.61	10.18	11.36	11.36	11.13	11.97
Na_2O	2.59	2.70	2.60	2.34	2.17	2.25	2.16	2.26	2.10	2.09	2.23	2.17	2.20	2.67	2.26	2.32	2.31	2.14
K_2O	0.65	0.67	0.62	0.57	0.53	0.54	0.50	0.52	0.50	0.49	0.51	0.48	0.50	0.67	0.53	0.55	0.54	0.55
TiO_2	3.12	3.37	3.18	2.84	2.60	2.70	2.61	2.70	2.56	2.43	2.62	2.56	2.66	3.28	2.72	2.77	2.64	2.63
P_2O_5	0.35	0.37	0.34	0.31	0.27	0.28	0.31	0.28	0.26	0.26	0.28	0.28	0.27	0.37	0.27	0.27	0.26	0.25
MnO	0.18	0.18	0.18	0.18	0.17	0.17	0.18	0.18	0.18	0.18	0.17	0.18	0.18	0.19	0.17	0.18	0.17	0.17
Total	100.00	100.00	100.00	100.00	100.00	100.00	100.00	100.00	100.00	100.00	100.00	100.00	100.00	100.0	100.00	100.00	100.00	100.0
Rb	10	11	11	9	8	–	7	10	11	9	9	8	11	11	9	11	9	5
Sr	418	428	408	386	363	–	350	372	361	344	365	348	369	423	427	413	399	371
Y	33	34	34	28	25	–	26	27	26	26	28	28	26	34	29	29	26	26
Zr	218	229	211	187	169	–	170	179	169	159	178	165	171	224	173	181	172	165
Nb	24	26	24	23	20	–	18	19	21	18	17	19	20	25	22	23	15	25
Ba	176	173	170	149	152	–	129	146	138	144	144	131	141	174	178	156	132	165
Ni	118	91	140	270	312	–	383	337	402	451	295	421	331	105	122	135	115	122
Cu	140	134	143	133	126	–	125	119	130	131	116	130	127	137	127	138	126	123
Zn	129	134	136	126	122	–	122	118	115	119	125	123	115	132	122	122	116	111
Cr	222	149	247	507	686	–	771	665	718	790	665	817	658	185	307	399	411	439
USNM[d]		.07	.12	.16	.18		.20	.21	.23	.24	.25	.26	.27					

NOTE:
[a] Data for the 1960 samples from Murata and Richter (1966; see also Table 1). Data are normalized to 100% after converting iron to FeO
[b] Data from Table A4. Normalized values (e.g., Rb n) are taken from the "Dec" columns
[c] Major oxide averages for 1952, 1961, and 1967 from Wright and Fiske (1971; see also Table 8); major oxide data for 1959 S-1 from Murata and Richter (1966, sample Iki-58). Trace element data from Table A4
[d] Numbers under which the samples are cataloged and stored at the U.S. National Museum, Washington D.C. (USNM 116112 number given in this row)

Lastly, some of the plagioclase phenocrysts are more sodic than the groundmass (microlitic) plagioclase present in the same glassy samples, again evidence that the early lavas are at least slightly hybrid. The mixing appears to have occurred within the magma chamber prior to eruption, without clear evidence for the admixture of hotter magma into the material being erupted; this type of mixing was also observed in the early 1955 lavas (Anderson and Wright 1972; Helz and Wright 1992).

When we compare the early 1960 lavas with the late 1955 lavas, which they so closely resemble, we see that conspicuous evidence for recent recharge and mixing in the 1955 magma chamber, documented for the late 1955 lavas in Helz and Wright (1992), has been largely obliterated. The plagioclase phenocryst population in the late 1955 lavas is bimodal in composition, whereas that in the early 1960 lavas is narrower, and more continuous in composition (Fig. 2). We interpret this narrowing of the range in plagioclase phenocryst composition in the early 1960 lavas as resulting from re-equilibration, followed by cooling and crystallization, during the 5 years between recharge and hybridization in 1955 and renewed eruption from the same chamber in 1960. In addition, the more forsteritic olivine phenocrysts and the coarse, complexly zoned augite phenocrysts seen in the late 1955 lavas are absent from the early 1960 samples we have examined. Again, we interpret this as the effects of very minor crystal settling, re-equilibration and renewed cooling and crystallization between 1955 and 1960.

The late 1960 lavas

The later 1960 lavas all contain very conspicuous evidence, not just for disruption and self-mixing of a previously hybridized, stored magma, but also for the influx of multiple pulses of more primitive magma and the incorporation of new differentiated magma into the stored body. The plagioclase phenocrysts are, almost without exception, resorbed and reversely zoned. The absence of euhedral overgrowths suggests that the resorption is quite recent. The restricted compositional range of plagioclase in the late 1960 lavas relative to the ranges observed in the early 1955, late 1955, and early 1960 lavas is consistent with a rise in the average temperature of the stored magma body, which is most reasonably attributed to the addition of hotter magma.

The augite phenocrysts frequently bear the marks of multiple reintrusion. One indicator is the appearance of progressively more magnesian rims on the phenocrysts, with each showing some signs of resorption before the new growth occurred (as in Figs. 4 and 6). The presence of some metastable subcalcic augite in the core of a sector-zoned augite (Figs. 6 and 7) provides evidence for recent, significant undercooling of at least part of the hotter component, during mixing of two magmas of different temperature. Similar features have been documented in augite phenocrysts in the late 1955 lavas (Helz and Wright 1992, their Figs. 4e and f, and pp 368–369), where they were also attributed to recent mixing of thermally disparate magmas.

The mere presence of augite and plagioclase in the late lavas is anomalous, because the late 1960 lavas all have bulk MgO contents well above the 7.0–7.5% at which augite and plagioclase begin to crystallize from Kilauean liquids; summit lavas of such compositions contain only olivine as a phenocryst. We suggest that these crystals have come from the lower part of a differentiated magma body, of which the early 1960 lavas represent the upper part. The overlap in augite compositions (Table A2) between the early and late 1960 lavas suggests that this slightly more crystal-rich lower layer was *not* much hotter than the upper part of the chamber prior to recharge.

The rare hypersthene reported in the early 1960 lavas (Richter and Murata 1966) must be xenocrystic to them, because the quenching temperature of all known early 1960 glasses (1122–1125 °C; see Table 5) is above hypersthene-in for Kilauean lavas (ca. 1090 °C; Helz and Thornber 1987; Helz 1987b). The hypersthene found in some of the late 1960 lavas is also clearly xenocrystic to its immediate host: It is resorbed and often rimmed with magnesian augite with which it is not in equilibrium, and is enclosed in glasses quenched from even higher temperatures than those in the early 1960 lavas.

The varying extent of augite overgrowth on hypersthene in the late 1960 samples provides strong evidence for repeated inmixing of highly differentiated liquids, similar in composition to the early 1955 lavas, during the latter part of the 1960 eruption. The occurrence of hypersthene + ilmenite confirms that one pocket of differentiated magma had reached a temperature of 1100 °C or less (Helz and Thornber 1987) by the time of its entrainment. The fact that the hypersthene in the late 1960 samples is slightly more Fe-rich than some of that in the early 1955 lavas is consistent with these pockets having undergone 5 more years of cooling and fractionation than had been achieved in 1955.

The olivine phenocryst population in the late 1960 samples, with its trimodal distribution of phenocryst-core compositions (Fig. 9) and convergent zoning (Fig. 10) strongly supports the idea that the late 1960 lavas are hybrids. Because olivine re-equilibrates fairly quickly, the preservation of the variant zoning patterns in crystals within single thin sections suggests that the mixing was recent. Following the arguments of Maaloe and Hansen (1982), it appears that some mixing events might have occurred only a few days before eruption and quenching, where the zoned margin is very narrow (Fig. 11A); the time gap would be longer, perhaps weeks to a few months in cases where the zoned margin is wider (Fig. 11B).

The presence of highly magnesian ($Fo_{87–89}$) olivine, both euhedral and kink-banded, provides direct evidence for the influx of primitive magma into the erupting chamber, as no olivine of this composition is pres-

ent in the 1955 or earlier 1960 lavas. The most magnesian olivine composition observed in the late 1955 lavas was $Fo_{84–85}$ (Helz and Wright 1992), which would be the liquidus olivine composition in a Kilauean melt containing at least 8.0–8.5% MgO, using the olivine-melt equilibrium data of Roeder and Emslie (1970). Using the same assumptions ($K_D = 0.30$; ferrous iron content of the melts 9.50–9.75%), the presence of euhedral $Fo_{87–89}$ olivine in the late 1960 lavas implies that their original host melts contained 12–13% MgO. Such melts would have quenching temperatures of 1255–1275 °C, much hotter than any of the observed glasses (see Table 1).

Glass compositions and quenching temperatures vs magma mixing

We have noted already the divergence between the glass compositions and bulk compositions in Fig. 13A, which is *prima facie* evidence for magma mixing. In this section we consider the implications of the inferred quenching temperatures of those glasses for the 1955 and 1960 eruption processes. The quenching temperatures of the early 1960 glasses are 1122–1125 °C; those inferred for glass and mesostasis compositions in the late 1955 samples are 1127–1132 °C. The sample base is small, but the difference in temperature is consistent with the early 1960 lavas having been produced by a hybridization event occurring in 1955, followed by 5–6 years of subsequent cooling and crystallization, during which (apparently) no further recharge occurred.

The composition of the late 1960 glasses gives a minimum estimate for the dominant postmixing temperature in the upper part of the magma chamber at the end of the 1960 eruption was 1142–1144 °C, 10 degrees below plagioclase-in (Thompson and Tilley 1969; Helz and Wright 1992), and 18–22° above the temperatures of the early 1960 melts. This rise in eruption temperature is consistent with considerable further recharge by hotter magma. Excavation of a zoned chamber is ruled out by the abundant petrographic evidence for very recent mixing, and by the paucity of melts of intermediate composition and temperature.

The contrast in glass composition (and quenching temperature) of the three lapilli in sample KP-26 implies additional complexity in the mixing process. This sample is described by Murata and Richter (1966) as having been collected at 8:30 p.m. on 18 February, and is apparently an observed fall. The three scoriae are all equally fresh, with no obvious evidence that one might have been erupted earlier than the other two. Two of the scoriae are among the hottest erupted; the third, differentiated scoria is cooler, but is hotter than the early 1960 pumices, and itself shows petrographic evidence of recent mixing. The heterogeneity suggests tapping of segmented chambers not recharged during the 1955 eruption, some of which had remained isolated throughout most of the 1960 eruption.

Magnesian recharge components of the later 1960 lavas

The variation in the 1960 lava compositions shown in Fig. 13 suggests that the magnesian lavas were produced by mixing a differentiated liquid that had undergone three-phase fractionation with a more magnesian liquid representative of magmas erupted at Kilauea's summit. Wright and Fiske evaluated this possibility with a series of mixing calculations (Table 11 of Wright and Fiske 1971), using average compositions for the early and late 1960 lavas. Several different summit magmas were tested; the best match involved three different summit compositions, 1959E[1] (lava from the early part of the 1959 eruption), 1961 (lava from the 1961 eruption in Halemaumau Crater), and 1967 (lava erupted from the 1967–1968 eruption of Halemaumau Crater). We have redone these calculations, taking each intermediate and late 1960 lava composition in turn, to verify the identity of the mixing components, and to look for systematic changes in their identity with time of eruption.

We use the following mixing equation for each sample erupted from 26 January to the end of the eruption, solving it by a least-squares method to identify the mixing components that yield the lowest residuals:

$$\text{Hybrid magma}(F-7 \text{ to } F-20) = 1960E + \text{Recharge magma (1952, 1961, 1967, 1959)} + \text{Olivine}(Fo_{90}, Fo_{70})$$

The 1960E composition is the average of the early 1960 lavas, and represents magma stored beneath the region of the 1960 vents prior to the beginning of the eruption. When lava compositions from eruptions earlier than 1952 or later than 1967 have been tested as possible recharge magmas, they have invariably resulted in unacceptably high residuals in one or more oxides, and/or negative mixing coefficients.

Diagnostic oxide and trace element characteristics for the preferred summit mixing components include the following:

Mixing component	Distinctive chemical components (compared at the same MgO content)
1952	high Al_2O_3, Sr; low Na_2O, K_2O
1961	low "FeO"; high Zr
1967–1968	low CaO, TiO_2, Nb
1959	high CaO; low Al_2O_3, Sr

The bulk compositions used are shown in Table 2. Each calculation was made with different combinations of these magmatic components until a solution was ob-

[1] The 1959E composition was calculated as an average of olivine-controlled lavas erupted early in 1959 (Wright and Fiske 1971; Table 8, footnote). Later, it was shown that the chemistry of all samples from the 1959 eruption could be expressed by adding variable amounts of olivine to the chemistry of samples S-1 and S-2, erupted respectively from the easternmost and westernmost vents active on the first day of eruption (Wright 1973). In the mixing calculations of this paper (Table 3 and Fig. 14) we use the chemistry of S-1, rather than 1959E.

Table 3a Results of major-oxide mixing calculations for the 1960 eruption

Sample no.[a]	F-7	F-8	F-9	F-11	F-12	F-13	F-14	F-16	F-17	F-18	F-19	F-20
Field No.	KP-13	KP-15	KP-17	KP-19	KP-20	KP-21	KP-22	KP-24	KP-25	KP-26	KP-27	KP-28
Date (1960)[a]	26 Jan	29 Jan	30 Jan	1 Feb	2 Feb	4 Feb	4 Feb	12 Feb	13 Feb	16 Feb	18 Feb	18 Feb
Active vent[b]	B	B	B	B	L	L	L	B	J	J	J	J
MgO content[a]	6.97	8.27	9.39	11.27	10.58	12.11	11.28	12.29	13.13	11.12	12.46	11.82
Mixing results												
1960E	86.3	55.4	49.4	32.0	41.2	34.1	42.5	39.8	33.9	38.2	44.4	49.2
1952	12.2	40.6	–	–	–	–	–	–	–	–	–	–
1961	–	–	43.9	57.1	49.3	50.1	39.3	–	–	–	–	–
1967–1968	–	–	–	–	–	–	–	32.7	33.5	31.4	14.5	12.0
1959 S-1	–	–	–	–	–	2.7	7.3	14.3	17.5	20.5	27.5	26.9
Olivine	1.5	4.0	6.7	10.9	9.5	13.1	10.9	13.2	15.1	9.9	13.6	11.9
(Fo content)	(84)	(88)	(84)	(85)	(85)	(85)	(86)	(87.5)	(87.5)	(88)	(87)	(88.5)
Residuals												
Largest	0.04	0.09	0.11	0.05	0.08	0.07	0.07	0.05	0.04	0.05	0.06	0.05
Average	0.02	0.02	0.02	0.02	0.02	0.03	0.02	0.02	0.02	0.02	0.02	0.02
MgO of magma added to 1960E[c]	11.1	10.7	12.5	13.7	13.6	15.2	15.0	16.3	16.7	14.2	17.4	17.2

[a] See Murata and Richter (1966; see also Table 2)
[b] See Richter et al. (1970)
[c] Calculated by combining olivine with olivine-controlled summit compositions in the proportions shown

Table 3b Trace element balances using the mixing solutions of Table 3a and the trace element contents in Table 2

Sample no.	F-7	F-9	F-11	F-13	F-14	F-16	F-17	F-18	F-19	F-20
Rb (2 s.d. = 4 ppm)										
obs.[a]	11	9	8	7	10	11	9	9	8	11
calc.[b]	10	10	10	9	9	8	8	8	7	8
Sr (2 s.d. = 11 ppm)										
obs.	408	386	363	350	372	361	344	365	348	369
calc.	417	390	371	361	369	351	342	363	348	***356***
Y (2 s.d. = 3 ppm)										
obs.	34	28	25	26	27	26	26	28	28	26
calc.	32	29	27	27	28	25	24	26	26	27
Zr (2 s.d. = 7 ppm)										
obs.	211	187	169	170	179	169	159	178	165	171
calc.	214	190	175	171	178	169	162	173	170	175
Nb (2 s.d. = 4 ppm)										
obs.	24	23	20	18	19	21	18	17	19	20
calc.	25	23	21	21	22	19	18	20	20	21
Ba (2 s.d. = 24 ppm)										
obs.	170	149	152	129	146	138	144	144	131	141
calc.	172	154	145	142	147	136	132	142	142	146
Ni (2 s.d. = 10 ppm)[c]										
obs.	140	270	312	383	337	402	451	295	421	331
calc.	137	***253***	***341***	384	337	***376***	***415***	***311***	***405***	***350***
Cu (2 s.d. = 8 ppm)										
obs.	143	133	126	125	119	130	131	116	130	127
calc.	***134***	128	123	119	121	***113***	***110***	117	***113***	***116***
Zn (2 s.d. = 6 ppm)[c]										
obs.	136	126	122	122	118	115	119	125	123	115
calc.	130	125	122	122	123	119	117	119	120	120
Cr (2 s.d. = 18 ppm)[c]										
obs.	247	507	686	771	665	718	790	665	817	658
calc.	252	512	686	755	667	***754***	***830***	652	***797***	***694***

NOTE! Calculated data shown in bold/italic (e.g., ***354***) differ from the observed by more than two standard deviations
[a] Data from Table 2
[b] Calculated from major oxide mixing solution given in Table 3a
[c] Calculated assuming the following chemistry for olivine (± chromite ± sulfide): 2114 ppm Ni; 3660 ppm Cr; 96 ppm Zn

tained with positive coefficients for all mixing components. (Negative coefficients are not physically meaningful, and the components with which they are associated are considered not relevant to the mixing process in question.) The Fo content of olivine in the mix is allowed to vary, as the least-squares program calculates whatever composition fits best, in the range Fo 90 to 70.

Two sets of calculations were tried; the first, as described above, used the early 1960 composition as the

starting point, in agreement with the petrographic evidence discussed previously. A second set was tried, in which the early 1955 composition was substituted for the early 1960 composition, in order to see how sensitive the results were to the composition of the stored component. This alternate set of calculations still required the same four recharge components, and in similar proportions and identical sequence. The only change was that the 1960E fraction was replaced by the combination 1955E + 1961, representing recharge of the 1955 magma chamber in calculations made previously (Table 11 of Wright and Fiske 1971).

The solutions with the lowest residuals are displayed in Table 3a and are shown in a bar graph series in Fig. 14. These solutions are well constrained, and the pattern seen in Table 2 is stable, even when the composition of the stored component is varied, as discussed above. Although small amounts (<10%) of rejected compositions cannot be ruled out, the solutions are distinctly worse when the components present in amounts greater than 10% are left out of the calculation. The calculated Fo contents of olivine are reasonable, falling within the range both of those observed in the 1960 olivines (see Fig. 9 and accompanying discussion) and those typical of lavas erupted at Kilauea's summit and east rift zone.

Three features of the results plotted in Fig. 14 stand out. Firstly, the compositions of the preferred inputs represent magmas erupted within a few years of 1960, i.e., those which could have been present in Kilauea's plumbing in early 1960. Secondly, the magnesian recharge magmas required by the least-squares solutions vary systematically when the hybrid compositions are plotted in their observed time sequence. Finally, the order in which recharge magmas are accepted as mixing components matches the order in which the magmas can be inferred to have arrived in the shallow Kilauea plumbing. These features of the results suggest that the mixing calculations are successfully modeling a real process, in which one recharge magma has followed another into the chamber which fed the later 1960 lavas.

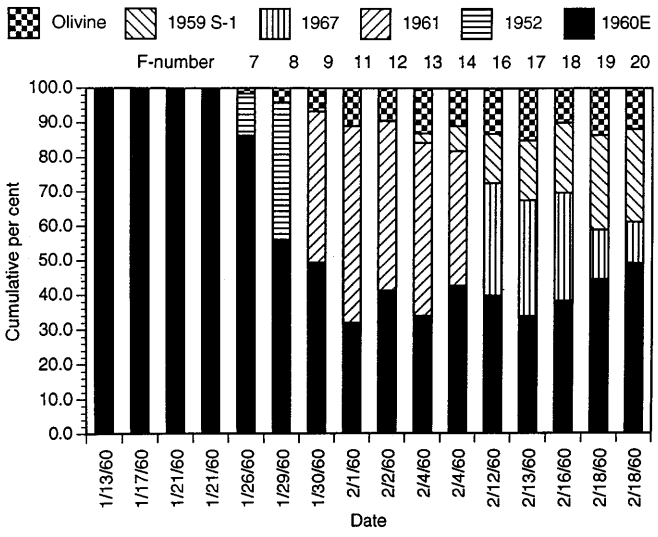

Fig. 14 Results of mixing calculations (Table 3a) for lavas from the 1960 eruption (see text for further explanation)

We are aware of the fact that it is possible to explain the chemical variation alone by fractionation of olivine, clinopyroxene, and plagioclase, as was demonstrated for the 1960 lavas by Russell and Stanley (1990, their Fig. 10, p 5034–5035). However, the petrographic evidence for mixing, and the large divergence between the sequence of 1960 bulk compositions and the actual 1960 Kilauean liquid descent line are more than sufficient to demonstrate that such calculations, no matter how successful mathematically, do not correspond to physical reality.

Trace element balances (Table 3b) are broadly consistent with the proposed mixing, with elements excluded from olivine, chromite, and sulfide in excellent agreement. Balances for the compatible elements (Cr, Ni, Cu) show minor discrepancies. We believe that the poorer fits for these elements reflect small variations in mineral composition and proportions [e.g., chromite/olivine ratios, variable nickel contents in olivine at the same Fo content (e.g., Clague et al. 1995, their Fig. 7, p. 313), and the presence of minor sulfide], rather than problems with the magmatic components chosen by the mixing calculations.

The variation of trace elements with MgO (Fig. 13B) illustrate the complexity of the mixing process. None of the four elements plotted for the hybrid samples follow an olivine control line (represented by the 1959 pair). Cr for some of the hybrid lavas falls slightly below any possible linear mixing trend, suggesting that some of the unfractionated magmas used as mixing components had lost chromite relative to olivine during storage at the summit and transport in the rift. This was also inferred to have occurred in the magnesian lavas which recharged the 1955 chamber (Helz and Wright 1992).

Temperatures of magmas involved in the mixing process

A minimum temperature of 1122–1125 °C for magma residing in the reservoir which fed the 1960 eruption is calculated from compositions of the early 1960 glasses (Table 1) using the calibration of Helz and Thornber (1987). After recharge during the 1960 eruption, glass temperatures as high as 1144 °C are observed. From the absence of phenocrystic plagioclase in several of the latest erupted samples, we can infer that the highest postmixing temperatures were closer to 1155 °C, the temperature at which plagioclase begins to crystallize in 1960 compositions (Thompson and Tilley 1969). The temperatures inferred from the glass compositions are 11–13 °C lower, and the glasses contain tiny microlites of plagioclase, consistent with the lower temperatures. Growth of groundmass crystals presumably occurred after mixing, most likely during eruption and subsequent cooling at the surface.

We have used the T_{MgO} values of the early 1960 glasses and the various later hybrids, plus the proportions of primitive and stored magmas taken from the mixing results (Table 2) to calculate a minimum temperature for the magmas added to the 1960 reservoir during the 1960 eruption (Table 4). The equation used is:

$$(X_{stored})(T_{stored}) + (X_{recharge})(T_{recharge}) = T_{hybrid}; \quad (1)$$

where X is the mass fraction of the magmatic components and T is the temperature. The only unknown is the temperature of the recharge magma. We assume that there are no nonideal heat-of-mixing effects when one Kilauean lava mixes with another, which seems reasonable, for such closely related melts.

Equation (1) applies when both stored and new components are crystallizing the same assemblage, in this case, the three-phase assemblage olivine + augite + plagioclase, which occurs below 1155 °C. However, for higher-temperature melts, crystallizing olivine only, the amount of heat released per degree is approximately 56% of that released during crystallization of the three-phase assemblage (Ghiorso 1985; Helz et al. 1993). If $T_{recharge}$ is >1155 °C, while T_{stored} is less, then an adjustment to $T_{recharge}$ is necessary. During mixing of magmas crystallizing the two different assemblages, the extra heat extracted from the hotter component is consumed remelting plagioclase ± augite in the cooler component. Therefore, if the initial temperature calculated for the recharge magma is above 1155 °C, we must adjust the result as follows:

$$T_{final} = 1155 + 1.78\,(T_{recharge} - 1155) \quad (2)$$

The results of these calculations are shown in Table 4 as T_{calc} (minimum).

The minimum temperature of the 1952 component mixed with the 1960 stored magma is 1144 °C, based on the mixing proportions obtained for sample KP-15 (F-8). This value may be low, as the glass in this sample is somewhat devitrified. The temperature of the 1961 component, based on sample KP-19 (F-11), is 1146 °C.

The other two components (1959 and 1967) are found only in combination. For these components we set up two equations of the form of Eq. (1) above, with two unknowns, and solved them simultaneously. The minimum temperature calculated for the 1959 component in KP-25, KP-26, and KP-27 (1172–1174 °C) is considerably hotter than 1155 °C (plag-in), and so was adjusted using Eq. (2). The minimum temperature of the 1967–1968 component is 1152–1154 °C, calculated from the data for the same three samples.

The late samples KP-25, KP-26, and KP-27 are those where the available thin sections lack any phenocrystic plagioclase. For these the temperature of the chamber immediately after mixing was arguably at least 1155 °C. Table 4 therefore includes the results of alternative calculations for the temperatures of the 1959 and 1967–1968 components, based on the assumption that the true temperatures at the time of mixing were 1155 °C. The resulting temperatures are 1239–1242 °C for the 1959 component and 1167–1169 °C for the 1967–1968 component. These temperatures represent the maximum inferable temperatures for these two components, consistent with the available petrographic and chemical data. The question is, Are these higher estimates still realistic, or are the minimum estimates based on actual glass compositions better?

We can evaluate the calculated temperatures of magma inputs by comparing them with the eruption temperatures estimated from glasses analyzed from the 1952, 1961, 1967–1968, and 1959 eruptions at Kilauea's summit and with liquidus temperatures calculated for bulk compositions of the samples from which glass was analyzed; these data are shown in Table 5. Our inter-

Table 4 Estimated temperatures (°C) for the various primitive components, required by least-squares calculations to make up the late 1960 lavas, assuming that the stored component had the composition and temperature of the early 1960 lavas

Sample no. (hybrid)	KP-15 F-8	KP-19 F-11	KP-25 F-17	KP-26 F-18	KP-27 F-19
Stored component	1960E	1960E	1960E	1960E	1960E
Weight fraction[a]	0.58	0.36	0.40	0.42	0.51
T_{MgO}	1123[c]	1123[c]	1123[c]	1123[c]	1123[c]
Hybrid					
T_{MgO} (Table 1b)	1133	1138	1144	1143	1142
T (plag-in)[b]	–	–	1155	1155	1155
Primitive component					
Type required	1952	1961	1967 + 1959	1967 + 1959	1967 + 1959
Weight fraction[a]	0.42	0.64	0.39 + 0.21	0.35 + 0.23	0.17 + 0.32
T_{calc} (minimum)	1144	1146	1154 + 1174[d]	1152 + 1172[e]	
T_{calc} (plag-in)			1169 + 1242[d]	1167 + 1239[e]	

[a] Weight fractions from Table 3a, renormalized to exclude olivine

[b] From Thompson and Tilley's (1969) experiments on 1960 lava compositions. Consistent with T_{MgO} values in Table 1b

[c] Average of early 1960 glasses (columns 1–5 in Table 1a)

[d] Calculated from solving simultaneous equations for mixing solutions for KP-27 and KP-25 (Table 3a)

[e] Calculated from solving simultaneous equations for mixing solutions for KP-27 and KP-26 (Table 3a)

Table 5 Composition and temperatures of glasses and bulk rocks from olivine-controlled eruptions at Kilauea's summit

Column no.	1	2	3	4	5	6	7	8
	1952 glass[a]	1961 glass[a]	1967 glass[b]	Ik-22 glass[c]	1952	1961[d]	1967	1959 S1
SiO_2	50.1	50.7	50.90	49.18	50.32	50.38	50.45	50.10
Al_2O_3	14.0	13.8	13.4	12.10	13.91	13.70	13.65	12.88
FeO (total)	11.30	10.8	12.00	11.33	11.32	10.83	11.26	11.21
MgO	6.91	6.99	6.44	10.03	7.14	7.64	7.60	8.11
CaO	11.3	11.20	10.8	11.17	11.36	11.36	11.13	11.97
Na_2O	2.36	2.49	2.68	2.33	2.26	2.32	2.31	2.14
K_2O	0.54	0.57	0.65	0.52	0.53	0.55	0.54	0.55
TiO_2	2.71	2.73	3.13	2.49	2.72	2.77	2.64	2.63
P_2O_5	0.26	0.26	0.23	0.22	0.27	0.27	0.26	0.25
MnO	0.18	0.19	0.18	0.13	0.17	0.18	0.17	0.17
Cr_2O_3	0.01	0.02	0.01	0.08	–	–	–	–
Sum	99.67	99.85	100.42	99.58	100.00	100.00	100.00	100.0
TMgO (glass)	1152	1154	1143	1216				
T_{MgO} (bulk)					1158	1168	1167	1177
Comments			Abundant, well-formed crystallites					

[a] Analyses from Helz et al. (1995)
[b] New data
[c] Hottest sample collected during the 1959 eruption and richest in the 1959E component (Table 25.4; in Helz 1987a). See text for further explanation
[d] Average of two samples, K-61-4 and K-61-22 (Richter et al. 1964)

pretations are limited by two factors:

1. All observed glass temperatures are minimum, because of imperfect quenching.
2. Each summit magma may have been thermally zoned in storage beneath Kilauea's summit, with the erupted fraction representing only the cooler, upper parts of the magma body.

The glass-quenching temperatures for samples from the summit eruptions in 1952 and 1961 are 1152 and 1154 °C, respectively (Table 5) and represent minimum temperatures for those magmas in storage beneath Kilauea's summit. The liquidus temperatures of the bulk compositions used in the calculations are 1158 and 1168 °C, respectively, and represent the maximum temperature of these components for which we have direct evidence. The inferred temperatures for 1952 and 1961 magmas that entered the 1960 chamber are close to the temperatures of the same magmas erupted at Kilauea's summit, given that the uncertainty in T_{MgO} is ±10 °C (Helz and Thornber 1987). If one accepts the results at face value, they suggest that the magma which recharged the chamber in 1960 was similar in temperature and composition to that erupted at the summit in 1952 and 1961.

The most magnesian glass erupted in 1959 has a quenching temperature of 1216 °C (Table 5 of Helz 1987a). This is well above the liquidus temperature of sample 1959 S-1 (1177 °C), which represents the 1959 component in the mixing calculations. The sample in which this most magnesian glass occurs, Iki-22 (sample S-5; Murata and Richter 1966), is itself a hybrid, containing 68% of the juvenile 1959 component and 32% of the stored 1959 component (Wright 1973; Helz 1987a). The temperature of the 1959 juvenile component in Iki-22, calculated using Eq. (1), is 1231 °C, assuming a glass quenching temperature of 1185 °C for samples consisting entirely of the stored 1959 component (Helz 1987a). The temperature of the 1959 juvenile component estimated from the 1960 samples (1239–1242 °C) and from Iki-22 (1231 °C) are remarkably close, given the assumptions involved in the calculations. Hence, we suggest that the higher temperatures are reasonable for this component. We mentioned previously that the presence of euhedral $Fo_{87–89}$ in some of the later 1960 lavas implied that those grains had crystallized, fairly recently, from magmas having temperatures of 1255–1275 °C; clearly, this would be the component most likely to be responsible for the presence of these olivines in the late 1960 lavas.

For the last component (the 1967 magma) the hottest actual spatter sample found for that eruption has glass with a quenching temperature of 1143 °C, and the liquidus temperature is 1167 °C (Table 5), both not unlike the value of 1152–1154 °C and 1167–1169 °C calculated as the minimum and maximum temperature for that component in Table 4. Thus, three of the four components identified by least-squares calculations as possible new inputs arrived with minimum temperatures of 1144–1154 °C, essentially identical to the temperatures as observed in the equivalent summit lavas (1143–1154 °C), within the uncertainty of the glass geothermometer (±10 °C; Helz and Thornber 1987). The fourth, the 1959 component, is distinctly hotter, and arrived crystallizing olivine only, regardless of which calculated result (1173 vs 1224 °C) we consider best. The most straightforward interpretation of these results, for all four components, is that transport of magma from the main reservoir to the east rift zone involves no

more cooling than transport from the reservoir to the surface at the summit.

Magnesia contents of the bulk compositions (olivine + liquid) added to the 1960 stored magma are tabulated in Table 3a. These range from just under 11 to nearly 18%. The temperatures calculated above for transport in the rift zone correspond to melt MgO contents of 6.5–10.3%, much lower than the magnesia contents indicated in the mixing calculations. The two sets of calculations can be reconciled if olivine was entrained during lateral transport in the rift zone.

Comparison of the 1955 and 1960 eruptions

The 1955 and 1960 eruptions were fed from the same reservoir complex underlying the easternmost subaerial part of Kilauea's east rift zone. To complete our interpretation of the 1960 eruption we contrast and compare events of 1960 with the events associated with the preceding 1955 eruption.

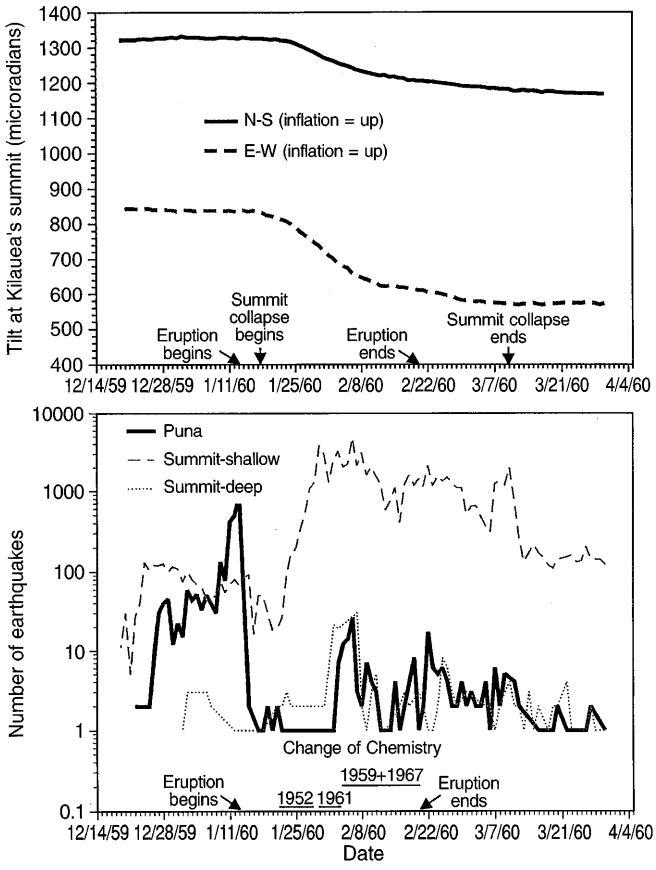

Fig. 15 Geophysical and geological observations made before, during, and following the 1960 eruption. *Top:* Tilting at Uwekahuna vault, Kilauea's summit, showing timing of summit collapse relative to beginning and end of eruption on the rift zone. *Bottom:* Seismicity at Kilauea's summit and near the site of eruption, compared with beginning and end of eruption and changes in chemistry during the eruption (see text for further explanation). Unpublished data, US Geological Survey Hawaiian Volcano Observatory. (Used with permission)

Eruption chronology

The chronology of events associated with the 1955 eruption were summarized in Part I (Helz and Wright 1992, their Table 1, Figs.1 and 2). The chronology of events preceding, accompanying, and following the 1960 eruption are shown in Fig. 15 and Table 6, extracted from the summary of Richter et al. (1970). The eruption began on 13 January and ended 5.5 weeks later, on 20 February. Eruption was initiated along a 1-km-long fissure northwest of Kapoho Crater (Fig. 1). Vents opened first down-rift, then up-rift (Richter et al. 1970, their Fig. 43), similar to the 1955 sequence. Later in the eruption, two additional vents opened within approximately 0.5 km to the east of the eastern end of the original line of vents. Temperatures, measured by optical pyrometer during the eruption, increased markedly on 31 January (Table 6; Richter et al. 1970, p. E58). The last 2 weeks of eruption were marked by steady, low-level activity without any obvious changes in the character of the effusion.

The 1960 eruption was preceded by several weeks of heightened seismic activity near the eventual site of eruption, culminating in an intense earthquake swarm (Fig. 15) and subsidence of the Kapoho Graben (Fig. 1) on the day before lava reached the surface. Five days after the eruption began, Kilauea's summit began to collapse; a delay between rift eruption and summit collapse also occurred in 1955. The collapse was accompanied by a swarm of long-period earthquakes beneath Kilauea's summit. Seismicity at the eruption site died out quickly, reaching background levels within a few days of the arrival of lava at the surface. During the eruption there was one short burst of increased seismicity lasting 2 days. Seismicity at Kilauea's summit gradually declined after the end of the collapse. Seismicity on the rift zone remained at background levels through the end of the eruption.

Essential features of the 1955 and 1960 eruptions are compared in Table 7. The two eruptions share the following characteristics:

1. Each eruption was preceded by several weeks of increasing seismicity near the eruption site, culminating in several days of felt earthquakes, ground cracking, and local subsidence.
2. Eruption began several days before collapse of Kilauea's summit.

The two eruptions also differ in the following important respects:

1. Resupply was more rapid in 1960, as evidenced by the shorter time separating summit collapse and change of eruption chemistry.
2. The 1960 eruption was more vigorous, as indicated by higher fountaining, with more olivine entrainment during mixing.

We infer from these data that the rift plumbing was more open in 1960 than in 1955, and that the travel of magma to the surface was more forceful and turbulent in 1960 than in 1955.

Table 6 Chronology of significant events during the 1960 eruption. [Eruption observations taken from Richter et al. (1970). Mixing chemistry taken from calculations presented in this paper (Table 3)]

Date (1960)	Active vents	Chemistry/field-temperature
1/13	Eruption begins at vents A–J	1960E
1/14	Vents B–E active; vent J sporadically active	
1/15	B now principal vent	
1/17		1960E
1/18	Highest fountaining of eruption	
1/21		1960E
1/24	Vent J reactivated	
1/26		1960E + 1952
1/27	New vents L and K open east of J	
1/29		1960E + 1952
1/30		1960E + 1961
1/31		Temperature increases from 1050–1080 to 1100 °C
2/1–3		1960E + 1961
2/4		1960E + 1961 + 1959
2/5	Rift line from E–H reopens; activity at L and B decreases	
2/6	Activity at L and B ceases; reactivated vents also decline	
2/7	Weak activity at B, E, and J to end of eruption	
2/12–18		1960E + 1967 + 1959
2/20	Eruption ends	

Table 7 Comparison of the 1955 and 1960 eruptions

Observations	1955	1960
Pre-eruption		
Seismicity beneath eruption site	Seismicity increased several weeks before eruption; intense seismic swarm 4 days before eruption	Seismicity increased several weeks before eruption; intense seismic swarm 1 day before eruption
Ground deformation near eruption site	Inflationary tilt change at Pahoa seismometer 4 days before eruption	Kapoho graben collapsed 1 day before eruption
During eruption		
Collapse of Kilauea's summit	7 days after eruption began	4 days after eruption began
Initial change of lava composition	13–18 days after summit collapse	5–8 days after summit collapse
Character of eruption		
Lava chemistry	Low MgO (5–7%)	High MgO (6–14%)
Temperature (glass MgO)	1099–1132 °C	1122–1144 °C
Fountain heights	30–130 m (average 50–60 m)	150–500 m (average 300 m)

Changes in mixing components related to eruptive events

In 1955, as documented by Helz and Wright (1992) and Wright and Fiske (1971), stored magma was hybridized, apparently by magma of 1952 composition, evident in lavas erupted approximately 2 weeks after the eruption began. During the eruption, magma of 1961 composition also moved from beneath Kilauea's summit to become the dominant component of the recharged reservoir which supplied magma to the 1960 eruption.

The pattern of mixing in 1960 is demonstrated by mixing calculations (Table 3a), ordered in Fig. 15 by the date of eruption. The only mixing components which yield low residuals in the mixing calculations have the chemistry of four summit lavas erupted within 10 years before or after the 1960 eruption. During the course of eruption the preferred magnesian recharge component changes systematically from one having the chemical peculiarities of the 1952 summit lava (26–29 January) through one having those of the 1961 summit lava (30 January to 4 February) to one having the character of the 1967 Halemaumau lava (12–18 February). The temporal sequence matches the order in which these compositions were erupted at Kilauea's summit.

One additional composition, 1959, becomes an important component of the mix beginning 4 February and remains so to the end of eruption. It appears with either the 1961 or 1967 components, as indicated.

Many of the compositional changes indicated by the mixing calculations can be correlated with specific events noted in the eruption chronology (Table 6). During the earliest part of the eruption, lava compositions suggest that only magma which had been hybrid-

ized in 1955 was actually erupted, although recharge of the chamber may have begun.

The first change of chemistry in the 1960 eruption occurred 1 week after Kilauea's summit began to collapse. The 1952 component (needed in samples KP-13 and KP-15; see Fig. 15) was already present in the rift zone, as it had been the early and dominant mixing component in 1955 (Table 6 of Helz and Wright 1992).

A temperature increase measured in the field (Table 6) and by increase of MgO in glass (Table 1a) correlates with opening of new vents east of the original curtain of fire, an increase in the ratio of juvenile to stored magma (KP-15; Table 3a) and a change in the recharge composition from 1952 to 1961 (sample KP-19; Table 3a). (Fountain temperatures obtained by optical pyrometry are known to be underestimated due to cooler material between the instrument and the source. Relative temperature increases or decreases are valid under comparable observing conditions. Temperatures obtained near this time from glass chemistry indicate that the field temperatures are approximately 35–40 °C too low.) The 1961 magma was also present in the rift, identified as the dominant magma introduced toward the end of the 1955 eruption (Wright and Fiske 1971). A further increase in temperature noted on 13 February (KP-25-27; Table 1a) followed a flurry of seismic activity near the eruption site on 4 February (Fig. 15) and the first appearance of the 1959 composition (Table 3a), the mantle derived component in the 1959 eruption (Helz 1987a).

Two independent lines of evidence are consistent with involvement of the 1959 magma in the 1960 eruption. We noted above that kink-banded olivines, singly or in aggregates, are observed in some of the late 1960 samples investigated. Kink-banded olivines are present in 5 of 7 samples which take the 1959 composition in the mixing solutions of Table 3. By contrast, equally magnesian 1960 lavas (F-11, F-12) which do not take the 1959 component do not have the deformed olivines. From the observations of Helz (1987a), this component of the 1959 eruption is the only known historic Kilauean summit magma to contain an abundance of kink-banded olivines. The association of the 1959 composition and this class of olivine in both the 1959 and 1960 eruptions suggests that there was something distinctive about the transport of this magma in Kilauea's plumbing. It may have moved faster than other magmas, whether vertically or horizontally, consistent with the very high temperatures observed and inferred for this component in both the 1959 and late 1960 lavas.

An additional piece of circumstantial evidence is contained in the report by Clague et al. (1995, p. 325) of a peculiar inclusion of hornfels-textured troctolite in a 1960 flow collected underwater off Cape Kumukahi. The host flow, dredged from the surface, would most likely be one of the latest flows to be erupted in 1960. Clague and coworkers (1995) interpreted the inclusion as coming from layer 3 of the oceanic crust under Kilauea. Xenoliths are extremely rare in Hawaiian tholeiitic lavas (Jackson 1968). It may be coincidental, but the 1959 magma, erupted immediately before the 1960 eruption, is one of the few other Kilauean lavas which contains xenolithic inclusions, some of which probably come from below the volcanic edifice (see discussion of annealed dunites in Helz 1987a).

The appearance of the 1967 component, in samples KP-24 through KP-28, is the most intriguing, as samples containing this component were erupted with no unusual rift events immediately preceding or accompanying the change in composition. Both of the hypersthene-bearing 1960 samples (KP-24, KP-26) require the 1967–1968 summit composition as a component of their make-up (Fig. 14), implying that the path traced by the 1967–1968 summit magma was offset from that of the 1952 and 1961 magmas responsible for previous mixing episodes in 1955 and 1960.

Additional calculations were made to test whether other mixing components (e.g., the 1955E chemistry instead of 1960E) obviated the need for the 1967 composition. In every case the residuals were unacceptably high when the 1967 component was absent. Inclusion of a small percentage of 1955E composition did not affect the residuals significantly, although the amount taken by the calculations is too small to be well constrained. We conclude that the 1967 component moved from beneath Kilauea's summit to the lower east rift zone by 1960, at least 2 years earlier than previous estimates (Wright et al. 1975; Wright and Tilling 1980; Wright and Heliker 1987). The calculated temperatures of mixing components summarized in Table 5 indicates that the 1967 component was hotter than the 1952 and 1961 components. This is consistent with its more recent appearance in the magmatic plumbing (i.e., 1960 compared with 1952 and 1955, respectively).

Mixing elsewhere in the east rift zone

Magma mixing has been documented chemically by Wright and coworkers for eruptions elsewhere on the east rift zone (Wright and Fiske 1971; Wright et al. 1975; Wright and Tilling 1980). More recently, Garcia et al. (1989; 1992) has made similar interpretations for the Puu Oo-Kupaianaha eruption of Kilauea which began in 1983, and Clague et al. (1995) have published a study of lavas erupted on the submarine part of Kilauea's east rift zone. The range of mineral compositions for the submarine lavas is shown in Table 8. The range of mineral compositions observed in the 1955 and 1960 lavas is almost as great as the total ranges of compositions for minerals in the submarine lavas, even though the latter cover lavas erupted over a long period of time and on a longer segment of the rift zone. Not surprisingly, abundant petrographic and chemical evidence for magma mixing is documented for the submarine lavas. We conclude that magma mixing is ubiquitous on Kilauea's east rift zone and is a necessary

Table 8 Comparison of mineral compositions (mol percent) in the 1955–1960 lavas with those collected from submarine lavas on Kilauea's east rift zone

Mineral	1955 lavas (Anderson and Wright 1972; Helz and Wright 1992)	1960 lavas (this paper)	Submarine lavas (Clague et al. 1995)
Olivine	Core $Fo_{76–85}$	Core $Fo_{76–88}$	Core $Fo_{78–91}$
Hypersthene	En_{75}	$En_{70–71}$	$En_{66–81}$
Augite	Mg/(Mg + Fe) = 0.83–0.69 Wo = 0.28 – 0.42	Mg/(Mg + Fe) = 0.84–0.74 Wo = 0.37–0.43	Mg/(Mg + Fe) = 0.84–0.66 Wo = 0.32–0.43
Plagioclase	$An_{51–78}$	$An_{57–80}$	$An_{47.7–81.3}$

consequence of the model for magma transport and storage presented in the final section of this paper.

Magma transport and storage at Kilauea

General model and the concept of magma batches

A broad framework for magma storage and transport at Kilauea has been developed from consideration of seismic and geodetic data. The distribution of magma beneath Kilauea's summit and upper east rift zone has been illustrated and discussed most comprehensively by Ryan (1988). Subsequent authors have confirmed and enlarged upon the great vertical extent of the rift magma plumbing (e.g., Delaney et al. 1990) and the presence of olivine cumulates at its base (Clague and Denlinger 1994). Our preferred interpretation of the rift plumbing, consistent with but not identical to those in the cited references, consists of three- tiers (Fiske et 1993). The uppermost tier, extending from the surface to depths of 3–4 km, has a high ratio of rock to magma. The middle tier (4–6 km) is the upper part of Ryan's aseismic "deep molten core." This tier is dominated by relatively crystal-poor magma. The lowest tier (6 km to the base of the volcanic pile at 10 km) is marked by increasing ratios of olivine to liquid, the deepest part corresponding to Clague and Denlinger's zone of dunite cumulate.

The upper zone is marked by intrusion of dikes, often accompanied by earthquake swarms (Klein et al. 1987). Many dikes reach the surface to feed eruptions; others do not and provide secondary bodies of stored magma which cool and crystallize, providing sources of fractionated liquids. The deeper parts of the rift zone are nearly aseismic (Klein et al. 1987).

Magma from the Earth's mantle enters Kilauea's shallow plumbing in batches of discretely different composition. A magma batch has been defined as a chemically distinctive group of lavas, from a single eruption, which are either uniform within analytical error or differ only by addition or subtraction of olivine (Wright 1971). The distinctive chemistry of the magma batches seen in 1952–1968 at Kilauea has provided a unique way of tracking movement of magma through

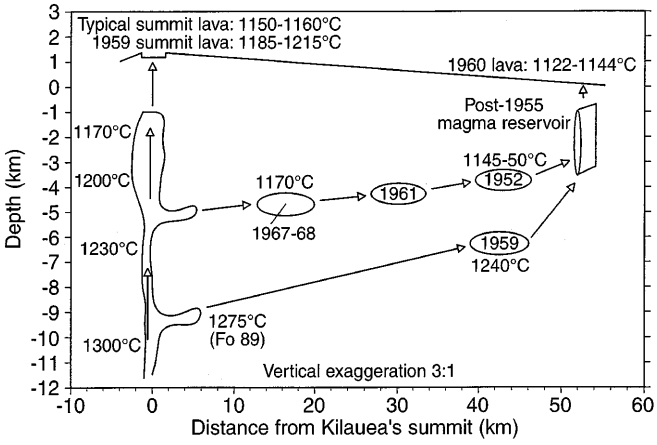

Fig. 16 Model for magma mixing in 1960. Temperatures on the left are estimated for magma moving upward from the mantle to supply Kilauea's shallow summit reservoir. The temperatures at the time of mixing in 1960 are given above *ovals* labeled with the composition of the various summit components involved in the mixing. The 1959 magma traveled along a deeper path than the other summit components. Approximately 60 °C of cooling occurs during storage before eruption at Kilauea's summit or east rift zone, regardless of the path traveled

the Kilauea plumbing, and led to the startling conclusion that a magma batch may appear in a hybrid lava erupted on Kilauea's east rift zone some years before it is seen in its unhybridized form at Kilauea's summit (Wright and Fiske 1971). The origin of inter-batch chemical differences is not known, but must be deeper than the shallow plumbing system, based on the observation that the chemistry of different batches cannot be related by fractionation of observed phenocrysts.

Model based on the 1960 eruption

Thermal structure of the rift plumbing

Figure 16 summarizes our inferences regarding the thermal structure of Kilauea's plumbing. Magma arrives from the mantle with a temperature at least as hot as 1300 °C (see also Clague et al. 1995). Cooling during storage at 2–6 km depth beneath Kilauea's summit re-

sults in a thermally zoned chamber whose top is approximately 1170 °C. We estimate that an additional 10–15° cooling usually occurs during upward transport to eruption at Kilauea's summit. Recharge of lower east rift reservoirs during the 1955 and 1960 eruptions was from magma that moved from the direction of Kilauea's summit unaccompanied by earthquakes directly associated with the transport path. The recharge magma arrived, as described above, at a temperatures similar to those observed in the corresponding eruptions at Kilauea's summit. These two facts argue very strongly that recharge occurs in a largely molten layer of the east rift zone, and that this zone retains a high temperature and a fluid connectivity along the entire distance, even during periods such as 1924–1952, when there is relatively little activity at Kilauea. These inferences are consistent with the geodetic evidence for a deep magma body within the rift zone (Ryan 1988; Delaney et al. 1990), as well as with the continuity of deep seismic activity on Kilauea's south flank, even in the absence of shallow rift intrusions or eruptions.

Water content and degassing of Kilauean magmas

A general model for degassing of Kilauea magma has been presented by Gerlach and Graeber (1985) and Greenland et al. (1985). These models have been applied to the origin of submarine lavas from Kilauea's east rift zone (Dixon et al. 1991; Clague et al. 1995). We cannot apply Dixon and Clague's model of mixing of undegassed and degassed magmas in the rift zone to the 1960 eruption, as we lack data on volatile contents in either lava glasses or in glass and fluid inclusions in minerals from the 1960 lavas. However, we can say that the volatile contents are low, as the phase relations for the 1960 lavas closely resemble those established for the Kilauea lava lakes. The derivation of internally consistent temperatures for magmas which had been erupted prior to 1960 and magmas not yet erupted makes it highly unlikely that the volatile contents of the different magmas used as mixing components differ significantly from each other or from the average volatile content of magma in shallow storage at Kilauea.

Rates of crystallization and cooling during storage in the east rift zone

It is possible using the results of the present study to further quantify the rate of crystallization of stored magma in the cooler upper tier of the rift zone. Wright and Tilling (1980) had inferred earlier that magma stored in the upper east rift, during a period when that segment of the rift had been very active, crystallized a three-phase assemblage of plagioclase-augite-Fe-rich olivine at a rate of 1–2% by weight per year. Model data for the late 1955 lavas (Table 2, average of Y and Z spatter from Wright and Fiske 1971) as compared with the early 1960 lavas (Table 2, average of F-1, -4, and -6) show approximately 8.1% crystallization by volume (8.5 % by weight) over the 5 years separating the two eruptions. As discussed above, the contrast in glass compositions between the late 1955 (1127–1132°; Table 2 of Helz and Wright 1992) and early 1960 glasses (1122–1125°; columns 1–5 in Table 1a), each of which lies in the three-phase crystallization regime, is consistent with cooling of 2–10 degrees over the 5-year interval between those eruptions. The crystallization and cooling rates can be related by thermodynamic modeling of the crystallization of Kilauean basalt (Ghiorso 1985), which yields 1–2.5 °C of cooling per year for three-phase crystallization and to 2–5 °C for crystallization of olivine ± chromite only (Helz et al. 1993). The various estimates of cooling and crystallization rates for magma stored in the east rift zone are mutually consistent.

Summary

The 1955 and 1960 eruptions demonstrate the importance of magma mixing within Kilauea's east rift zone and provide constraints on magma transport and storage at Kilauea. Kilauea magmas arriving from the mantle are stored before eruption in a reservoir located 2–6 km beneath Kilauea's summit. One component of the 1959 eruption in Kilauea Iki crater apparently followed a different path, arriving at the surface without intersecting Kilauea's summit reservoir and at a much higher temperature than that of most Kilauea eruptions. Three different lavas originating from Kilauea's summit reservoir traveled to the lower east rift zone in 1955 and 1960 to mix with cooler magma already stored there. The 1959 component was erupted in hybrid lavas late in the 1960 eruption, and likewise appears to have been much hotter than the other summit components mixed in 1960.

We estimate that most magma feeding rift eruptions leaves the main conduit near the base of shallow storage, approximately 5–6 km beneath Kilauea's summit. Magma progresses aseismically through the fluid core of the rift zone, cooling as it moves away from the summit. During intrusions magma moves upward from the main rift conduit into the upper few kilometers of the rift zone and becomes isolated from the main transport path. The reservoir which fed the 1955 and 1960 eruptions represent one such intrusion. The intruded magmas cool, crystallize, and differentiate at a rate of approximately 1–2% by weight per year. As in 1960 they may be intersected at any time by hotter magmas moving from the main rift conduit to the surface, thus producing eruptions in which magma mixing is important.

The amount of cooling that a magma undergoes in summit storage and between the summit reservoir and the point of eruption, i.e., transport through the summit reservoir or through the main east rift conduit, averages approximately 60 °C, regardless of the path taken.

The temperature at the time of eruption or mixing just prior to eruption may vary with time in storage, hotter magmas having spent less time in storage.

Appendix

Table A1 Compositions of plagioclase in 1960 spatter samples

Column no.	1	2	3	4	5	6	7	8	9	10
Field no.	KP-4	KP-4	KP-22	KP-22	KP-22	KP-22	KP-24	KP-26	KP-26	KP-28
Type	Microphenocrysts		Resorbed	Euhedral average	Phenocryst		Inclusions	Phenocryst		Inclusions
Grain	Cores	Rims			Core	Tip		Core	Tip	
No. of points	5	4	6	9	3	1	3	4	1	4
SiO_2	52.3	52.9	52.0	49.1	50.7	48.1	51.8	51.0	48.6	48.9
TiO_2	–	–	–	–	–	–	–	–	–	–
Al_2O_3	30.2	29.5	30.6	32.2	31.5	32.9	30.4	31.1	32.8	32.2
ΣFeO	0.73	0.97	0.64	0.71	0.65	0.88	0.78	0.69	0.75	0.92
MnO	–	–	–	–	–	–	–	–	–	–
MgO	0.15	0.22	0.12	0.23	0.24	0.23	0.17	0.20	0.23	0.16
CaO	13.40	12.29	13.13	14.95	14.28	16.02	13.35	13.93	15.25	15.05
Na_2O	3.51	3.95	3.58	2.54	2.93	2.18	3.47	3.12	2.32	2.83
K_2O	0.12	0.14	0.12	0.07	0.09	0.07	0.10	0.09	0.06	0.08
Sum	100.41	99.97	100.19	99.80	100.39	100.38	100.01	100.13	100.01	100.14
An (mol %)	67.5	62.6	66.5	78.5	72.9	79.9	67.6	70.7	78.2	74.2
Ab (mol %)	31.9	36.6	32.8	21.2	26.6	19.8	31.8	28.8	21.6	25.2
Or (mol %)	0.6	0.9	0.7	0.3	0.5	0.3	0.6	0.6	0.3	0.6

1–2: Average core and rim compositions for normally zoned, euhedral, lathy plagioclase microphenocrysts in early 1960 pumice
3: Unzoned, strongly resorbed plagioclase phenocryst in late 1960 pumice, illustrated in Fig. 3A
4–6: Reversely zoned, euhedral plagioclase phenocryst, from same section as feldspar in column 3
7: Average composition of inclusions in the resorbed, reversely zoned olivine shown in Fig. 11A
8–9: Composition of slightly resorbed and reversely zoned plagioclase phenocryst in the more differentiated scoria in sample KP-26
10: Average composition of inclusions in a resorbed, reversely zoned olivine phenocryst in sample KP-28

Table A2 Compositions of pyroxenes and ilmenite in 1960 spatter samples

Column no.	1	2	3	4	5	6	7	8	9	10
Field no.	KP-4	KP-4	KP-24	KP-24	KP-24	KP-24	KP-24	KP-24	KP-24	KP-24
Type	Augite	Augite	Opx	Augite	Ilmenite	Opx	Augite	Augite	Augite	Augite
Grain	Core	Rim		Rim	In opx		Core	Rim 1	Rim 2	Darkest
No. of points	3	2	3	2	2	4	6	3	4	5
SiO_2	51.1	50.9	53.2	51.9	0.00	52.6	50.8	50.8	51.8	52.7
TiO_2	1.04	1.08	0.61	0.95	45.6	0.67	1.40	1.06	0.89	0.62
Al_2O_3	2.17	2.74	1.39	2.71	0.00	1.28	2.39	2.21	2.49	1.58
Cr_2O_3	0.39	0.67	0.08	0.66	0.21	0.00	0.00	0.07	0.62	0.40
ΣFeO	8.49	7.18	16.4	7.25	46.8	16.4	10.2	9.61	6.85	6.49
MnO	0.21	0.19	0.34	0.18	0.30	0.25	0.18	0.18	0.10	0.17
NiO	0.05	0.07	–	–	–	0.03	0.02	0.01	0.05	0.01
MgO	16.9	16.5	25.2	17.8	6.25	25.9	16.0	17.2	17.5	18.9
CaO	19.0	20.2	2.36	18.7	0.00	2.28	18.9	18.7	19.6	18.9
Na_2O	0.23	0.22	0.03	0.26	0.00	0.00	0.24	0.21	0.17	0.10
Sum	99.56	99.75	99.67	100.41	99.16	99.41	100.13	100.05	100.07	99.87
En (mol %)	47.9	47.1	69.8	50.5		70.5	45.3	47.8	49.4	52.3
Fs (mol %)	13.4	11.5	25.5	11.5		25.0	16.2	15.0	10.8	10.0
Wo (mol %)	38.7	41.4	4.7	38.0		4.5	38.5	37.2	39.8	37.6

(Continued)

Table A2 Continued

Column no.	11	12	13	14	15	16	17	18	19
Field no.	KP-25	KP-25	KP-25	KP-26	KP-26	KP-26	KP-28	KP-28	KP-28
Type	Augite	Subcalcic augite	Augite core	Opx	Augite core	Augite rim		Augite phenocryst	
Grain	Dark sector		Light sector		Core	Rim		Core	Rim
No. of points	6	2	6	8	2	1	7	5	3
SiO_2	51.2	53.8	49.4	53.8	50.7	51.6	51.2	51.7	51.5
TiO_2	1.02	0.59	1.33	0.66	1.36	1.03	0.94	0.93	0.95
Al_2O_3	2.34	1.03	3.78	1.02	2.97	2.49	2.58	1.85	2.41
Cr_2O_3	0.02	0.02	0.30	0.05	0.27	0.51	0.74	0.21	0.66
ΣFeO	8.29	11.2	7.87	16.7	8.32	7.73	0.67	8.4	7.31
MnO	0.15	0.20	0.16	0.30	0.20	0.15	0.16	0.22	0.18
NiO	0.01	0.00	0.01	0.07	0.10	0.12	0.08	0.06	0.07
MgO	17.6	23.0	16.9	25.4	16.4	17.3	16.7	17.1	17.6
CaO	19.8	10.5	19.7	2.37	19.6	19.4	20.6	19.0	18.8
Na_2O	0.18	0.05	0.16	0.05	0.26	0.25	0.25	0.24	0.26
Sum	100.42	100.37	99.65	100.42	100.18	100.58	99.52	99.71	99.74
En (mol %)	48.2	62.3	47.6	69.7	46.6	48.6	47.7	48.2	49.9
Fs (mol %)	12.8	17.2	12.5	25.7	13.3	12.2	10.0	13.3	11.7
Wo (mol %)	39.0	20.6	39.9	4.6	40.1	39.2	42.3	38.5	38.4

1–2: Core and rim composition for augite microphenocryst in KP-4; crystals is next to olivine phenocrysts in Table A3, columns 1 and 2
3: Hypersthene in cluster shown in Fig. 8A
4: Augite rim on hypersthene in cluster shown in Fig. 8A
5: Ilmenite inclusion in hyperstehene (Fig. 8A)
6–10: Compound grain shown in Fig. 4. Compositions in columns 8–11 taken along line of traverse marked in that figure. Augite in column 11 is from darkest area adjacent to opx lamella
11–13: Sector-zone augite from sample KP-25 shown in Fig. 6. Compositions taken along line of traverse
14–16: Hypersthene xenocryst (Fig. 8B) and augite microphenocrysts from differentiated scoria in sample KP-26 (see glass analysis in column 5 in Table 1b)
17: Euhedral augite phenocryst (unzoned) in sample KP-28
18–19: Reversely zoned augite with phantom sector zoning (but no preserved compositional differences) in sample KP-28

Table A3 Compositions of olivine in 1960 spatter samples

Column no.	1	2	3	4	5	6	7	8	9
Field No.	KP-4	KP-4	KP-22	KP-24	KP-24	KP-25	KP-25	KP-25	KP-25
Type	Euhedral		Deformed	Euhedral		Olivine fragment		Deformed	
Grain	Core	Rim		Core	Rim	Core	Rim	Core	Rim
No. of point	3	2	3	4	3	4	2	3	1
SiO_2	39.2	38.9	40.9	39.4	39.0	38.9	38.6	40.5	40.1
TiO_2	0.02	0.02	0.02	0.04	0.05	0.01	0.02	0.06	0.07
Al_2O_3	0.04	0.04	0.00	0.02	0.01	0.06	0.06	0.00	0.00
Cr_2O_3	0.03	0.03	0.10	0.02	0.06	0.03	0.04	0.07	0.04
ΣFeO	17.9	20.3	11.9	20.5	18.0	20.2	18.1	13.6	15.8
MnO	0.23	0.26	0.19	0.28	0.27	0.29	0.27	0.19	0.20
NiO	0.31	0.18	–	0.15	0.22	0.25	0.28	–	–
MgO	41.6	39.6	46.1	39.6	41.5	40.2	41.8	44.6	43.5
CaO	0.21	0.25	0.25	0.23	0.30	0.28	0.32	0.28	0.31
Na_2O	0.02	0.03	0.00	0.00	0.02	0.03	0.02	0.04	0.03
Sum	99.56	99.61	99.46	100.24	99.43	100.22	99.45	99.34	100.05
Fo (mol %)	80.6	77.7	87.3	77.5	80.4	78.0	80.5	85.4	83.0

1–2: Olivine phenocryst from early sample KP-4. Euhedral, normal zoning
3: Cores of several olivines from the cluster of deformed olivines illustrated in Fig. 12
4–5: Resorbed reversely zoned olivine in KP-24, shown in Fig. 11A. Black rectangles are plagioclase inclusions. (Composition given in column 7 in Table A1)
6–7: Inclusion-rich fragment of olivine from KP-25, shown in Fig. 11B
8–9: Deformed olivine in KP-25; this grain is right next to the Fe-rich olivine fragment (columns 6 and 7). The glass surrounding these two grains is shown in Table 1b, columns 1 and 2

(Continued)

Table A3 Continued

Column no.	10	11	12	13	14	15	16
Field no.	KP-26	KP-26	KP-26	KP-26	KP-26	KP-28	KP-28
Type	Deformed		Euhedral			Resorbed	
Grain	Core	Rim	Core	Rim		Core	Rim
No. of points	6	1	5	2	4	4	1
SiO_2	40.2	39.5	38.8	39.1	38.8	38.7	38.6
TiO_2	0.02	0.05	0.04	0.04	0.08	0.01	0.03
Al_2O_3	0.08	0.00	0.04	0.03	0.05	0.07	0.09
Cr_2O_3	0.10	0.04	0.02	0.03	0.03	0.02	0.03
ΣFeO	11.9	16.8	21.6	19.5	22.1	21.7	19.3
MnO	0.19	0.28	0.27	0.25	0.27	0.29	0.23
NiO	0.32	–	0.18	0.20	0.10	0.21	0.29
MgO	46.7	42.6	39.3	40.8	38.6	39.0	41.5
CaO	0.30	0.28	0.26	0.32	0.27	0.28	0.36
Na_2O	0.02	0.04	0.04	0.02	0.02	0.02	0.02
Sum	99.83	99.59	100.55	100.29	100.32	100.30	100.42
Fo (mol %)	87.3	81.9	76.4	78.9	75.6	76.2	79.3

10–11: Olivine xenocryst in hot scoria in sample KP-26 (glass composition shown in Table 1b, column 3)
12–13: Euhedral, reversely zoned olivine microphenocryst in hot scoria in sample KP-26
14: Olivine microphenocryst in differentiated scoria in sample KP-26 (glass analysis shown in Table 1b, column 5)
15–16: Resorbed, coarsely skeletal (?) olivine, with plagioclase inclusions, from sample KP-28. Inclusion compositions shown in Table 1b, column 10

Table A4 Trace element data for the 1960 and related eruptions

Sample	Eruption	May Rb n	Dec Rb n	May Sr n	Dec Sr n	May Y n	Dec Y n	May Zr n	Dec Zr n	May Nb n	Dec Nb n
52-5-32	1952		9		427		29		173		22
Iki-22	1959E	6	6	285	284	19	18	122	119	17	16
Iki-58	1959E		5		371		26		165		25
F-01	1960	13	10	424	418	29	33	211	218	24	24
F-06	1960	12	11	420	428	31	34	222	229	22	26
F-07	1960	14	11	417	408	30	34	214	211	25	24
F-09	1960	11	9	378	386	26	28	183	187	19	23
F-11	1960	11	8	365	363	24	25	173	169	20	20
F-13	1960	12	7	358	350	24	26	175	170	20	18
F-14	1960	8	10	362	372	25	27	175	179	17	19
F-16	1960	9	11	349	361	25	26	166	169	19	21
F-17	1960	8	9	341	344	24	26	160	159	20	18
F-18	1960	10	9	363	365	25	28	173	178	20	17
F-19	1960	9	8	348	348	25	28	165	165	17	19
F-19GL	1960	11	10	393	412	27	30	189	192	21	21
F-20	1960	8	11	360	369	24	26	170	171	20	20
K-61-01	1961		14		420		30		180		23
K-61-17	1961		11		416		30		183		21
K-61-22	1961		9		404		27		180		24
HM68-02	1967	10	9	374	392	23	27	166	171	15	17
HM68-15	1967	10	9	400	407	27	24	173	173	17	14
	SD (%)[a]	12		1.5		4		2		9.9	
	SD (ppm)[a]	2		5		2		4		2	

NOTE: Samples were analyzed by XRF twice, in May and December, 1989, and values were normalized to standard sample BHVO-1, analyzed at the same time. The normalized data (e.g., Rb n) are tabulated in this table. The December analyses are used in Tables 2 and 3b.
[a] Standard deviations are calculated for replicated analyses of the same sample done at the same time. The values given are the average for all samples replicated and are used to estimate the precision of analysis. The intra-sample variation is not known. The upper row gives the analytical precision as a percentage of the average value of the analyzed element; the lower row gives the analytical precision in parts per million

(Continued)

Table A4 Continued

Sample	Eruption	May Ba n	Dec Ba n	May Ni n	Dec Ni n	May Cu n	Dec Cu n	May Zn n	Dec Zn n	May Cr n	Dec Cr n
52-5-32	1952		178		122		127		122		307
Iki-22	1959E	106	110	985	731	134	126	119	120	1486	1586
Iki-58	1959E		165		122		123		111		439
F-01	1960	168	176	127	118	145	140	135	129	204	222
F-06	1960	166	173	103	91	146	134	141	134	144	149
F-07	1960	148	170	159	140	148	143	135	136	229	247
F-09	1960	152	149	372	270	140	133	129	126	444	507
F-11	1960	142	152	421	312	134	126	126	122	656	686
F-13	1960	126	129	532	383	128	125	122	122	686	771
F-14	1960	134	146	483	337	130	119	117	118	618	665
F-16	1960	135	138	538	402	127	130	119	115	681	718
F-17	1960	126	144	622	451	126	131	122	119	732	790
F-18	1960	136	144	377	295	120	116	121	125	614	665
F-19	1960	140	131	544	421	114	130	124	123	728	817
F-19GL	1960	144	173	137	132	129	135	122	123	338	377
F-20	1960	131	141	394	331	110	127	113	115	590	658
K-61-01	1961		165		141		140		123		431
K-61-17	1961		157		131		143		126		381
K-61-22	1961		145		133		130		118		386
HM68-02	1967	121	147	126	115	125	126	127	115	345	413
HM68-15	1967	130	119	129	116	125	126	123	118	347	409
	SD (%)[a]	3.5		2.7		3		3		3	
	SD (ppm)[a]	12		5		4		3		9	

Acknowledgements We thank M. Garcia for providing unpublished microprobe data for plagioclase phenocrysts in the 1955 lavas. David Clague and Elizabeth Moll-Stalcup made thorough and incisive reviews of an early version of the manuscript. S. Maaloe, M. Carroll, and an anonymous reviewer also contributed significantly to improving the final interpretations and their presentation.

References

Anderson AT (1976) Magma mixing: petrological process and volcanological tool. J Volcanol Geotherm Res 1:3–33

Anderson AT, Wright TL (1972) Phenocrysts and glass inclusions and their bearing on oxidation and mixing of basaltic magmas, Kilauea volcano, Hawaii. Am Mineral 57:188–216

Clague DA, Denlinger RP (1994) Role of olivine cumulates in destabilizing the flanks of Hawaiian volcanoes. Bull Volcanol 56:425–434

Clague DA, Moore JG, Dixon JE, Friesen WB (1995) Petrology of submarine lavas from Kilauea's Puna Ridge, Hawaii. J Petrol 36:299–349

Delaney PT, Fiske RS, Miklius A, Okamura AT, Sako MK (1990) Deep magma body beneath the summit and rift zones of Kilauea Volcano, Hawaii. Science 247:1311–1316

Dixon JE, Clague DA, Stolper EM (1991) Degassing history of water, sulfur, and carbon in submarine lavas from Kilauea Volcano, Hawaii. J Geol 99:371–394

Eichelberger JC (1975) Origin of andesite and dacite: evidence of mixing at Glass Mountain in California and at other circum-Pacific volcanoes. Geol Soc Am Bull 86:1381–1391

Fiske RS, Swanson DA, Wright TL (1993) A model of Kilauea Volcano's rift-zone magma system (abstract). Eos, Trans Am Geophys Union (Suppl) 74:646

Garcia MO, Ho RA, Rhodes JM, Wolfe EW (1989) Petrologic constraints on rift-zone processes. Bull Volcanol 52:81–96

Garcia MO, Wolfe EW, Ulrich GE, Ho RA (1992) Petrology of lavas from episodes 2–47 of the Puu Oo eruption of Kilauea Volcano, Hawaii: evaluation of magmatic processes. Bull Volcanol 55:1–16

Gerlach TM, Graeber EJ (1985) Volatile budget of Kilauea volcano. Nature 313:273–277

Ghiorso MS (1985) Chemical mass transfer in magmatic processes I. Thermodynamic relations and numerical algorithms Contrib Mineral Petrol 90:107–120

Greenland P, Rose WI, Stokes JB (1985) An estimate of gas emissions and magmatic gas content from Kilauea Volcano. Geochim Cosmochim Acta 49:125–129

Helz RT (1987a) Diverse olivine types in lava of the 1959 eruption of Kilauea Volcano and their bearing on eruption dynamics. U.S. Geol Surv Professional Paper 1350 1:691–722

Helz RT (1987b) Differentiation behavior of Kilauea Iki lava lake, Kilauea Volcano, Hawaii: an overview of past and current work. Magmatic processes: physicochemical principles. Geochem Soc Spec Publ 1:241–258

Helz RT, Thornber CR (1987) Geothermometry of Kilauea Iki lava lake, Hawaii. Bull Volcanol 49:651–668

Helz RT, Wright TL (1992) Differentiation and magma mixing on Kilauea's east zone. Bull Volcanol 54:361–384

Helz RT, Hon K, Heliker C (1993) Thermal efficiency of lava tubes at Kilauea Volcano, Hawaii. In: IAVCEI General Assembly on Ancient Volcanism and Modern Analogues, Canberra, Australia, Sept 1993 (abstract):p. 47

Helz RT, Banks NG, Heliker C, Neal C, Wolfe EW (1995) Comparative geothermometry of recent Hawaiian eruptions. J Geophys Res 100:17637–17657)

Ho RA, Garcia MO (1988) Origin of differentiated lavas at Kilauea Volcano, Hawaii: implications from the 1955 eruption. Bull Volcanol 50:35–46

Jackson ED (1968) The character of the lower crust and upper mantle beneath the Hawaii Islands. In: 23rd International Geological Congress, Prague, 1968. 23rd Proc Int Geol Congr sec 1, Upper mantle (geological processes), pp 135–150

Klein FW, Koyanagi RY, Nakata JS, Tanigawa WR (1987) The seismicity of Kilauea's magma system. U.S. Geol Surv Professional Paper 1350 2:1019–1185

Maaloe S, Hansen B (1982) Olivine phenocrysts of Hawaiian olivine tholeiite and oceanite. Contrib Mineral Petrol 81:203–211

Macdonald GA, Eaton JP (1964) Hawaiian volcanoes during 1955. US Geol Surv Bull 1171:1–170

Murata KJ, Richter DH (1966) Chemistry of the lavas of the 1959–1960 eruption of Kilauea volcano, Hawaii. US Geol Professional Paper 537-A:A1–A26

Rhodes JM, Dungan MA, Blanchard DP, Long PE (1979) Magma mixing at mid-ocean ridges: evidence from basalts drilled near 22°N on the Mid-Atlantic ridge. Tectonophysics 55:35–61

Richter DH, Murata KJ (1966) Petrography of the lavas of the 1959–1960 eruption of Kilauea volcano, Hawaii. US Geol Surv Professional Paper 537-D:D1–D12

Richter DH, Ault WU, Eaton JP, Moore JG (1964) The 1961 eruption of Kilauea Volcano, Hawaii. US Geol Surv Professional Paper 474-D:D1–D34

Richter DH, Eaton JP, Murata KJ, Ault WU, Krivoy HL (1970) Chronological narrative of the 1959–1960 eruption of Kilauea volcano, Hawaii. US Geol Surv Professional Paper 537-E:E1–E73

Roeder PL, Emslie RF (1970) Olivine-liquid equilibrium. Contrib Mineral Petrol 29:275–289

Ross M, Huebner JS (1979) Temperature-composition relationships between naturally occurring augite, pigeonite, and orthopyroxene at one bar pressure. Am Mineral 64:1133–1155

Russell JK, H Stanley CR (1990) Origins of the 1954–1960 lavas, Kilauea Volcano, Hawaii: major element constraints on shallow reservoir magmatic processes. J Geophys Res 95:5021–5047

Ryan MP (1988) The mechanics and three-dimensional internal structure of active magmatic systems: Kilauea Volcano, Hawaii. J Geophys Res 93:4213–4248

Thompson RN, Tilley CE (1969) Melting and crystallisation relations of Kilauean basalts of Hawaii. The lavas of the 1959–1960 Kilauea eruption. Earth Planet Sci Lett 5:469–477

Wright TL (1971) Chemistry of Kilauea and Mauna Loa lava in space and time. US Geol Surv Professional Paper 735:1–40

Wright TL (1973) Magma mixing as illustrated by the 1959 eruption, Kilauea volcano, Hawaii. Geol Soc Am Bull 84:849–858

Wright TL, Fiske RS (1971) Origin of the differentiated and hybrid lavas of Kilauea volcano, Hawaii. J Petrol 12:1–65

Wright TL, Heliker CC (1987) Magma storage and differentiation in the Kilauea east rift zone prior to the Puu Oo eruption (January 1983–present). In: Geol Soc Am 83rd Annual Meeting, Cordilleran Section, Hilo, Hawaii, 20–22 May, abstracts with programs, p. 465

Wright TL, Swanson DA, Duffield WA (1975) Chemical compositions of Kilauea east-rift lava, 1968–1971. J Petrol 16:110–133

Wright TL, Tilling RI (1980) Chemical variation in Kilauea eruptions 1971–1974. Am J Sci 280-A:777–793